BALLISTIC FLASH CHARACTERIZATION OF ENTRY-SIDE FLASH

THESIS

David J. Peyton, BS

AFIT-OR-MS-ENS-12-21

DEPARTMENT OF THE AIR FORCE
AIR UNIVERSITY

AIR FORCE INSTITUTE OF TECHNOLOGY

Wright-Patterson Air Force Base, Ohio

The views expressed in this thesis are those of the author and do not reflect the official policy or position of the United States Air Force, Department of Defense, or the United States Government.

AFIT-OR-MS-ENS-12-21

BALLISTIC FLASH CHARACTERIZATION OF ENTRY-SIDE FLASH

THESIS

Presented to the Faculty

Department of Operational Sciences

Graduate School of Engineering and Management

Air Force Institute of Technology

Air University

Air Education and Training Command

In Partial Fulfillment of the Requirements for the

Degree of Master of Science in Operations Research

David J. Peyton, BS

February 2012

AFIT-OR-MS-ENS-12-21

BALLISTIC FLASH CHARACTERIZATION OF ENTRY-SIDE FLASH

David J. Peyton, BS

Approved:

_____//SIGNED//_____	5 Sep 2012
Dr. Raymond R. Hill (Chairman)	date
_____//SIGNED//_____	5 Sep 2012
Darryl K. Ahner, LTC, USA (Member)	date
_____//SIGNED//_____	5 Sep 2012
Mr. Jaime J. Bestard (Member)	date

Abstract

Aircraft survivability is a broad subject that encompasses many fields and subjects. An important part of aircraft survivability is fire prevention. Flashes created by ballistic impacts are a very real threat to aircraft because they can start fires or cause explosions. In an effort to better protect against these flashes, this study seeks to further the understanding and characterization of them.

Recent research on this subject has been greatly helped by the use of high-speed video footage of flash events. This footage has led to new algorithms and methodologies for how to characterize a flash. A preliminary predictive model of a flash event has already been made, but needs to be refined before implementation. This research effort is dedicated to further refining and developing this predictive model by finding a new time series model that more aptly describes the shape of the analyzed data. To this end, new data have been created and analyzed, and a new predictive flash model has been created. This model has been validated and proven to be adequate. Even though there is some amount of work that can still be done to enhance it, it is recommended that this model be implemented into the current flash prediction tools.

To my Mother and Father who have always been supportive

Acknowledgements

My thanks go out to my faculty advisor, Dr. Raymond Hill for his unwavering support and subtle but effective guidance of this thesis effort. I have been privileged to work with such an astute mentor.

I would also like to thank the sponsor unit, the Survivability Analysis Flight of the 46th Test Group, for their support of this research by collecting and processing all of the data. In particular, I would like to thank Mr. Jaime Bestard who was instrumental in making sure we were always heading in the right direction.

Table of Contents

List of Figures

List of Tables

List of Equations

BALLISTIC FLASH CHARACTERIZATION OF
ENTRY-SIDE FLASH

1. Introduction

1.1. Background

Aircraft survivability studies encompass a wide variety of projects designed to further the understanding of what causes damage to and destroys aircraft. These studies allow designers to make predictions on how survivable an aircraft will be. These predictions lead to more informed decisions in aircraft design and use which, in turn, hopefully lead to less battlefield casualties and more cost savings in aircraft design.

One major part of aircraft survivability is the analysis of incoming projectiles. Incoming projectiles come in countless varieties, but two primary types are armor piercing incendiary (API) rounds and fragments from exploding missile warheads. API rounds are specifically designed to penetrate and burn while warhead fragments are simple steel shards that are nevertheless very dangerous to aircraft. Kinetic energy from incoming steel fragments can deform and penetrate aircraft materials. At high speeds, the energy given off from the fragment can even cause the oxidation of the target and small flakes of the fragment dispersed by an impact (spall). This oxidation of the target and spall causes relatively small, but very intense, flashes to occur. Figure 1.1 shows a rough illustration of flashes created by an incoming fragment.

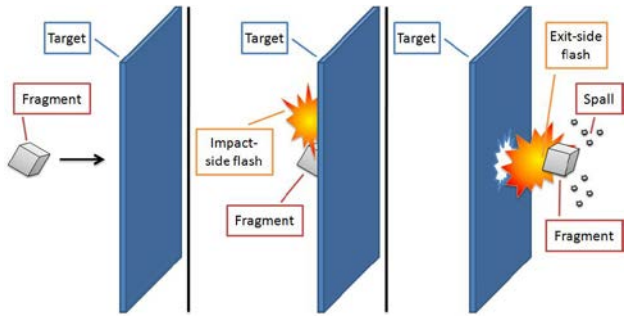

Figure 1.1 Illustration of a Ballistic Impact Flash [2]

These flashes may be far less extensive than those created by API rounds, but they are capable of igniting any flammable liquids present. This presents an obvious threat to aircraft survivability. Explosions or fires from such a flash igniting any on board liquids could be catastrophic for an aircraft.

The 46th Test Group, Survivability Analysis Flight at Wright Patterson Air Force Base has worked for years studying ballistic penetrations. They analyze these types of flash events using high-speed video. Analysis of this video is done in an attempt to characterize the flash by using the initial parameters of the shot. Past studies have focused on five aspects of the shot: initial projectile velocity, projectile size, target material type, target thickness, and the angle of obliquity between the shot line and the target.

1.2. Problem Statement

Previous work by Henninger (2010) and Talafuse (2011) have created a preliminary entry-side flash model for predicting the size, shape, position and orientation of the flash at any given time based on the initial parameters of the shot. This preliminary model and the methodology upon which it is based still need to be refined and further developed in order to create a more accurate entry side flash model. The

Henninger (2010) time series model used by Talafuse (2011) was somewhat questionable in its validity. Use of a new time series model for the flash event could create more accurate results when combined with Talafuse's (2011) methodology of creating a meta-model based on the initial parameters of the shot.

In addition, the datasets used in previous research efforts have been hampered by small size and unusable data. A new designed experiment which corrects these problems is necessary to fully flesh out the properties that have a significant impact on the flash event.

2. Literature Review

This chapter provides information on the foundations of the current research effort. The basis for this effort starts with a series of four AFIT theses written from 1991-1993. These theses provide insight into how ballistic impact flashes were characterized in the past. From there, this chapter examines the more current work that has been done on the subject. Bestard and Kocher (2010) created a mathematical algorithm allowing them to collect data on flash size and position based on high speed video footage of flash events. Both Henninger (2010) and Talafuse (2011) helped refine this data collection method in their research. Henninger (2010) attempted to describe the size of a flash with respect to time. Talafuse (2011) then worked towards expanding this model in order to describe and the size and duration of a ballistic impact flash based on the characteristics of the target panel and impacting projectile. Lastly, this chapter describes the basic aspects of survivability analysis, and the particular tools that are of interest to this research effort.

2.1. Reynolds 1991

Reynolds [9] studied the incendiary functioning (IF) of Soviet armor piercing incendiary (API) projectiles impacting graphite/epoxy composite panels. Until his effort, most studies had concentrated on metal targets. Reynolds used multivariate analysis and response surface methodology to reveal a negative correlation between projectile residual mass and incendiary functioning.

Before Reynolds' research, most vulnerability assessments relied on a government study from the 1960s called Project THOR. This study showed that target material and projectile characteristics (weight, speed, angle, etc.) were both important

factors in determining projectile penetration. One limitation of the study was that it did not examine incendiary or high explosive effects [9].

Based on Project THOR's results, the Joint Technical Coordinating Group for Munitions Effectiveness (JTCG/ME) published the Penetration Equations Handbook for Kinetic-Energy Penetrators. This handbook is used to determine whether or not an API round will function based on the target material. The handbook has five different levels of incendiary functioning: Incendiary fails to function, functions completely, partially functions, slow-burns, or has a delayed function. If a projectile or material was not tested, correction factors can be applied to the equations to account for the difference. Unfortunately, these correction factors are not accurate for describing the effects of composite materials.

In an effort to update this handbook, Reynolds analyzed test data of Soviet 12.7mm API rounds fired at different angles against various composite material thicknesses. API rounds are specifically designed to ignite flammable liquids in their targets by having a metal jacket over incendiary material. On impact with the target, the metal jacket is intended to penetrate the target and peel away exposing and igniting the incendiary material underneath. If the round punctures hydraulic or fuel lines, the flammable liquids contained in those lines may be ignited by the incendiary material.

The four predictor variables that Reynolds used to derive formulas for residual mass (RM), residual velocity (RV) and incendiary function (IF) were impact velocity (IV), impact mass (IM), ply thickness (PLY), and impact obliquity angle (ANG). Reynolds also derived models for two types of IF. Type I indicated an entry-side functioning that could ignite fuel, while for Type II was classified as a non-function. The

regression equations that resulted produced a numerical result which was rounded into one of the following 5 categories:

0 - No Function

1 - Delayed Function

3 - Slow Burn

4 - Partial Function

5 - Complete Function

Reynolds research expanded on JTCG/ME so that it included composite targets, but still left room for improvement in regards to the classification of incendiary functioning.

2.2. Knight 1992

Knight [6] re-examined the past work and sought to create a better model for residual velocity, residual mass and incendiary function of an API projectile. He used regression analysis, discriminant analysis, and neural networks to analyze data from 12.7mm and 14.5mm API rounds impacting graphite/epoxy composite panels.

Wright Laboratories Survivability Enhancement Branch ran the tests used for Knight's study. Out of the tests run, 281 shots were deemed valid for analysis of IF. The experiment used high-speed flash photography to document IF, and separated the IF for each shot into one of three classifications:

#1: 2-group classification (nonfunctioning and functioning)

#2: 2-group classification (nonfunction (entry-side functions included) and mixed)

#3: 3-group classification (entry-side, nonfunctions, and mixed)

The mixed category included complete, delayed, slow burn, and partial functioning shots [6].

Knight found a neural network algorithm the best method for classifying each shot into one of three categories: frontal (entry side function), mixed functioning (includes all types of function), and nonfunctions. The classifications he used were approximate values based on expert observation of the shot results, but were not specific in terms of flash size or duration.

2.3. Lanning 1993

Lanning [7] expanded Knight's work by examining the impact of API projectiles on two composite panels. Lanning only examined IF in relation to the residual projectile mass and found that IF was not a quantifiable variable. Technology available at that time made studying IF an inexact science where it was typically categorized into one of seven categories: non-function, partial, slow burn, frontal, delayed, complete and total. These categories are similar to what Knight observed in that they were very approximate measurements.

Because Lanning was studying impacts on two panels, the possible results of the IF were expanded. However, with only 52 data points to work with, he reduced the number of IF categories to two. Like Knight, Lanning also found neural networks to yield promising results. He also noted that composite panels require a higher projectile velocity to produce flashes, and that the flashes produced had a longer duration than those associated with aluminum panels.

2.4. Blythe 1993

Blythe [4] was one of the first to study flashes produced by metallic impact on a target. His study concentrated mostly on the residual velocity and residual mass of the projectile, but also attempted to find a correlation to the exit-side flash produced by the impact. Blythe mentions similar work done previously by Ritter in 1986 and 1989, but notes that studies on exit-side flashes have not been done much prior to that time.

Blythe's study used steel fragments fired from 20mm and 30mm guns impacting aluminum and composite targets. He studied three different impact velocities between 4,000 fps and 10,000 fps. He observed exit-side flashes on the aluminum panels starting with the mid-velocity shots (~7,000 fps) and on the composite panels only with the high-velocity shots (~10,000 fps). Blythe noted that the flashes from the aluminum panels peaked much more quickly than the composite panel flashes (0.2 milliseconds compared to 1.1 milliseconds). Blythe did not make any type of flash model, but did recommend that future studies on exit-side flashes for composite panels concentrate on the 7,000-9,000 fps range to determine a more exact minimum velocity for flash generation.

2.5. Bestard and Kocher 2010

Recent, technological advances allow for capturing ballistic impact flashes on high-speed video yielding a frame rate conducive to image processing. Using this new technology, Bestard and Kocher [2] used image processing algorithms to enclose the flash inside an ellipse which they accomplish on a frame-by-frame basis. Figure 2.1 shows an example of an encapsulating ellipse produced by this process. Because of the inherent noise of the flash, they used a numerically stable method based on least squares minimization to create the ellipse for each flash. Measurement data from each ellipse

provides an estimate of the flash position, size (in X and Y coordinate dimensions) and orientation as a function of time for the duration of the flash.

Figure 2.1 Video Frame with Entry and Exit Flashes and Fitted Ellipses [2]

Given a set of n boundary data points ($\vec{x}_i$ and $\vec{y}_i$), the definition of an ellipse is

$$F(x,y) = p_1x^2 + p_2xy + p_3y^2 + p_4x + p_5y + p_6 = 0, p_2^2 - 4p_1p_3 < 0$$

Bestard & Kocher [2] expressed the ellipse-specific fitting problem as a constrained minimization problem

$$\min_{\vec{a}} \|\boldsymbol{D}\vec{a}\| \text{ subject to } \vec{a}^T\boldsymbol{C}\vec{a} = 1$$

where

$$\boldsymbol{D} = \begin{bmatrix} \tilde{x}_1^2 & \tilde{x}_1\tilde{y}_1 & \tilde{y}_1^2 & \tilde{x}_1 & \tilde{y}_1 & 1 \\ \vdots & \vdots & \vdots & \vdots & \vdots & \vdots \\ \tilde{x}_n^2 & \tilde{x}_n\tilde{y}_n & \tilde{y}_n^2 & \tilde{x}_n & \tilde{y}_n & 1 \end{bmatrix}, \vec{a} = \begin{bmatrix} \vec{a}_1 \\ \vec{a}_2 \end{bmatrix}, \vec{a}_1 = [p_1 \quad p_2 \quad p_2], \vec{a}_2 = [p_4 \quad p_5 \quad p_6]$$

and

$$\boldsymbol{C} = \begin{bmatrix} \boldsymbol{C}_1 & \boldsymbol{0} \\ \boldsymbol{0} & \boldsymbol{0} \end{bmatrix}, \boldsymbol{C}_1 = \begin{bmatrix} 0 & 0 & 0 \\ 0 & -1 & 0 \\ 2 & 0 & 0 \end{bmatrix}$$

The optimal solution of the system corresponds to the eigenvector of $\vec{a}$.

This algorithm provides a time series of ellipse positions (S), sizes (A), and orientations (φ) for each test event whose parameters are given by:

$$S(t_i) = \sqrt{x_{0,i}^2 + y_{0,i}^2}, A(t_i) = \pi r_{x,i} r_{y,i}, \text{and } \varphi(t_i) = \frac{1}{2} arccot\left(\frac{p_1 - p_3}{p_2}\right)$$

where:

$$x_{0,i} = \frac{2p_3p_4 - p_2p_5}{4\beta},$$

$$y_{0,i} = \frac{2p_1p_5 - p_2p_4}{4\beta},$$

$$r_{x,i} = \sqrt{\frac{\alpha}{\beta(p_3 - p_1) - \gamma}},$$

$$r_{y,i} = \sqrt{\frac{\alpha}{\beta(p_1 - p_3) - \gamma}},$$

and:

$$\alpha = \frac{1}{2}(p_1p_5^2 + p_3p_4^2 + p_6p_2^2 - p_2p_4p_5 - 4p_1p_3p_6),$$

$$\beta = \left(\frac{p_2^2}{4} - p_1p_3\right)\sqrt{1 + \frac{p_2^2}{(p_1 - p_3)^2}},$$

$$\gamma = (p_3 + p_1).$$

Bestard and Kocher tried to generalize the overall displacement and flash size. They concluded that the components of the flash trajectory (i.e., the x and y components) were hard to establish, but that the overall displacement (S) generally follows a logarithmic trajectory [2]. They observed that fragment flashes on the impact side show rapid growth and slower decay while exit side flashes exhibit slower growth and decay. Data were collected on the magnitude of the major radius and minor radius for entry-side

flash, where the major radius is the semi-major axis and the minor radius the semi-minor axis of the ellipse. No function was fit to these components; however, Bestard and Kocher noticed that the function for a Weibull distribution closely resembles the time series of the data describing the overall area of the flash cloud for an entry-side flash.

Bestard and Kocher also concluded that orientation of the flash clouds are not clear and with orientation ranges between 0° and 90°, the most plausible simplification of these variations is to consider a constant orientation, found by taking the average of the orientation time series [2].

The subsequent efforts use the flash data generated by the Bestard and Kocher image processing methods to create predictive models of the flash event.

2.6. Henninger 2010

Henninger [5] used the algorithm developed by Bestard and Kocher to create a time-based empirical model of a flash event. Henninger examined test data from eight selected shots of steel fragments against bismaleidmide resin (BMI) targets collected by the 46th Test Group, Survivability Analysis Flight. Based on previous research, Henninger's designed experiment varied four factors: projectile weight, projectile velocity, target panel thickness, and impact angle of obliquity. He focused on analyzing both the X-axis and the Y-axis radii of the entry-side flash. Based on this analysis, he found that a quartic model provided a good fit to the flash radius over time, as seen in Figure 2.2.

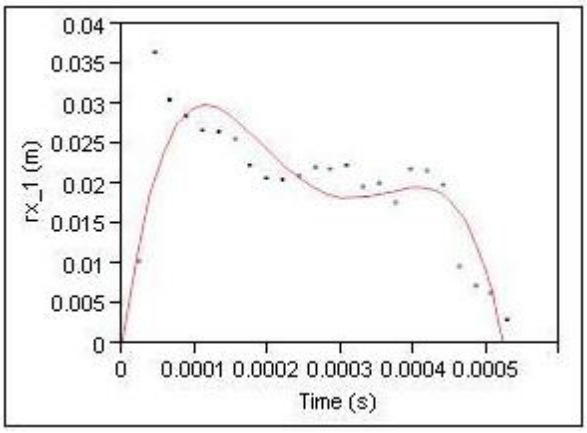

Figure 2.2 Quartic Fit of X-Radius vs. Time

This model takes the form

$$r_{x_i}(t) = x_1 t + x_2 t^2 + x_3 t^3 + x_4 t^4 + x_i \tag{2.1}$$

$$r_{y_i}(t) = y_1 t + y_2 t^2 + y_3 t^3 + y_4 t^4 + y_i. \tag{2.2}$$

Henninger also combined replicates with the same design settings and fit a quartic model to these combined data sets. He found that these models had an averaging effect between the two replicates and was not as accurate in modeling the flash radius. This can be seen in Figure 2.3. He also combined data sets across projectile weights, with similar results.

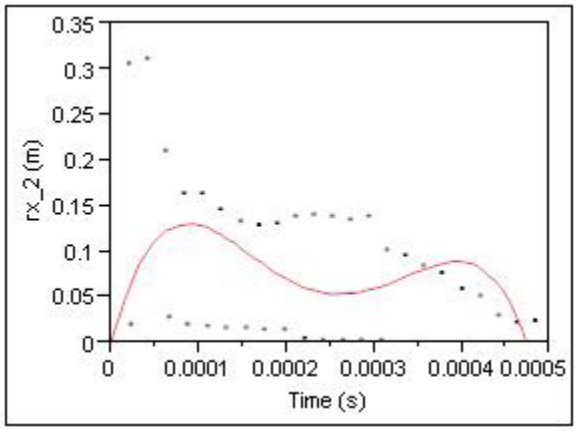

Figure 2.3 Combined Model: X-Radius vs. Time

Henninger concluded that aggregating the data added to the error but did not add to the fidelity of the model. Henninger also found that the residuals of the model had non-constant variance and were not normally distributed. This led Henninger to suggest that a better model for the flash radius would be of the form

$$FlashRadius = f(time) + g(time) \tag{2.3}$$

where $g(time)$ represents the error in terms of a time series model [5]. He did not investigate the $g(time)$ component in his work.

2.7. Talafuse 2011

Talafuse [10] attempted to expand Henninger's quartic model so that it could be used to predict the size, shape and position of the entry side flash over time based on the parameters of the incoming projectile. Talafuse introduced the concept of a meta-model that would predict the coefficients of Henninger's time dependent model based on the parameters of the incoming projectile. Talafuse intended the meta-model to predict all four coefficients of the quartic model (β_i) based on the velocity of the incoming projectile, the thickness of the target panel, the mass of the incoming projectile, and the angle of obliquity between the shotline and the target panel. His initial meta-model equation is included below:

$$\beta_i = b_0 + b_1(Thickness) + b_2(Angle) + b_3(Mass) + b_4(Velocity), i = 1, \dots, 4 \tag{2.4}$$

where each $b_0,\dots,b_4$ are specific to each β_i, and where

$$FlashRadius(time) = \beta_1 t + \beta_2 t^2 + \beta_3 t^3 + \beta_4 t^4. \tag{2.5}$$

Talafuse based his model on the analysis of 72 shots of steel projectiles at bismaleidmide resin targets. Unfortunately, in the majority of the shots, the image left the screen before the flash was complete, thus censoring the processed data. Only 21 of

the 72 shots were usable for analysis due to these difficulties. When the resulting reduced dataset was analyzed, panel thickness was found to be the only significant parameter in predicting the flash model. This changed the original meta-model equation to a simplified version:

$$\beta_i = b_0 + b_1(Thickness), i = 1, \dots, 4. \tag{2.6}$$

The resulting model predicted the flash radius with a fair amount of accuracy as shown below in Figure 2.4:

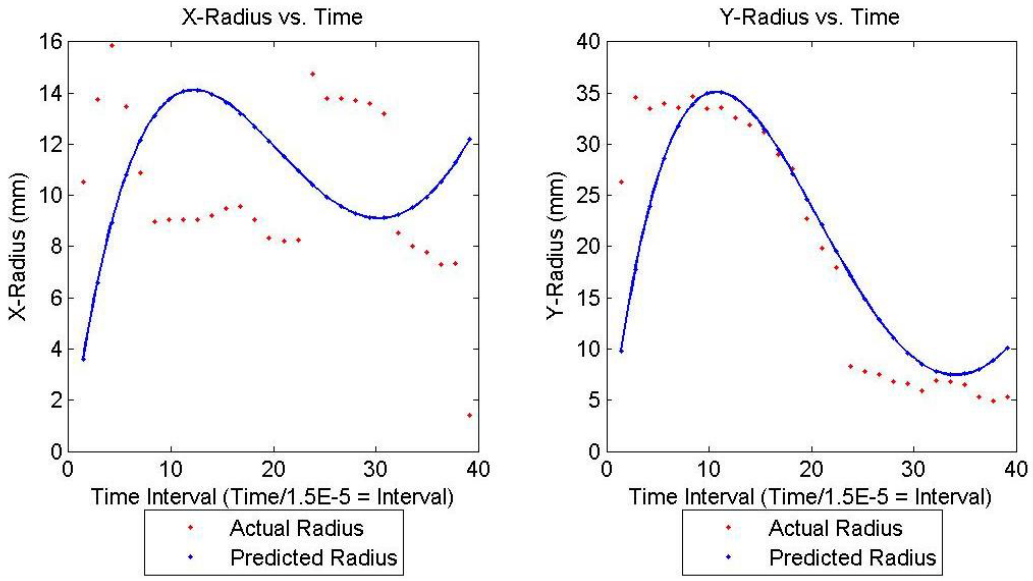

Figure 2.4 Predicted vs. Actual Radius Comparison for One Shot of Talafuse Model [10]

Note that the behavior of the flash model in Figure 2.4 depicts growth of the flash later in the duration versus the observed dissipation. This undesirable behavior was more pronounced in the current research effort, and is addressed in the next chapter.

2.8. Survivability Analysis

Survivability analysis, in general, studies how vulnerable designs of vehicles are to damage. For aircraft this involves studying a multitude of different parameters that

relate to two different probabilities: the probability of the aircraft being hit, and the probability of the aircraft being destroyed or disabled given that it has been hit [1]. These probabilities are then used in simulations of battle scenarios to better understand the limitations and uses of aircraft. The specific survivability models that the current research effort is being used in are the FPM and the COVART model.

2.9. COVART

The Computation of Vulnerable Area Tool (COVART) model predicts the ballistic vulnerability of vehicles (fixed-wing, rotary-wing, and ground targets), given ballistic penetrator impact. Each penetrator is evaluated along each shotline (line-of-sight path through the target). Whenever a critical component is struck by the penetrator, the probability that the component is defeated is computed using user defined conditional probability-of-component dysfunction given a hit (Pcd/h) data. COVART evaluates the vulnerable areas of components, sets of components, systems, and the total vehicle. In its simplest form, vulnerable area is the product of the presented area of the component and the Pcd/h data. The total target vulnerable area is determined from the combined component vulnerable areas based upon various target damage definitions.

COVART can model several penetrators: a single missile fragment, a set of missile fragments, a single Man Portable Air Defense (MANPAD) missile, a single Armor Piercing Incendiary (API) projectile, and a single High Explosive Incendiary (HEI) projectile. COVART can also model the damage mechanisms induced by threat penetrators. Damage is modeled using several methods. Analysts' selection of the damage mechanism modeling method depends upon the penetrator type and failure modes of the equipment being modeled. Physical damage criteria, such as hole size or damage

distance, are preferred because they can be directly related to live tests. Distance criteria are used to model blast and hydrodynamic ram induced damage. Hole size criteria is used to model functional failures due to liquid leaking from a container. Air-gap distance criteria are used to model sustained fires from threat induced leaks of flammable materials. Other equipment damage is modeled using penetrator impact mass and velocity relationships. A given component may be vulnerable to several damage effects. The COVART model uses failure analysis trees (fault trees) to assess the cascading effects of damage. The fault trees use data obtained from ground simulators (flight controls simulators, hydraulic system simulators, avionics coolant simulators, fuel system simulators, electrical power simulators) to enhance the robustness and quality of failure predictions.

COVART requires data characterizing the threat; velocity, material etc. The model also needs specific data on the materials and thicknesses of aircraft components. Required inputs for the critical components, for the kill level being analyzed, include Pcd/h data and fault tree data for redundant components. The COVART model assumes the penetrator or fragment travels along the shotline, ricochet and spall are not modeled, and blast effects are not considered. The COVART model determines the component and aircraft vulnerable areas as a function of the kill level for the specified attack directions. Numerous kill levels can be modeled [1].

2.10. FPM

The Fire Prediction Model (FPM) is an engineering tool used by COVART that predicts the probability and characteristics of a fire produced by a ballistic impact. It simulates the events that occur when a ballistic projectile penetrates a vehicle and

impacts a container holding a flammable liquid. It includes a library of common risks such as API and high explosive incendiaries, as well as sparks and hot surfaces. FPM also includes fluid properties for many types of jet fuel and hydraulic fluids and even models fire suppression agents [3].

2.11. Summary

Early studies of ballistic impact flashes were hampered in large part by a lack of sufficient video technology to capture the flash. As such, early studies focused more on classifying the type of flash to predict the type of flash produced for incoming projectiles.

The more current work uses high-speed video technology along with the ellipse generating algorithm developed by Bestard and Kocher (2010) to create data of the actual size and shape of ballistic impact flashes over time. This flash data was then analyzed to characterize and predict the size, shape and position of the flash over time based on the parameters of the incoming projectile.

The next chapter describes the current methodology of how these ballistic impact flashes can be characterized and presents a new model for predicting these flashes.

3. Methodology

This chapter details the overall methodology of the current research effort. It starts with how the data was collected using a similar but slightly improved method. It then goes on to detail the analysis effort where the previous model suggested by Talafuse (2011) was examined and later replaced by the current model. Lastly it describes the validation methods used to ensure that the current model is an improvement on the current flash prediction algorithms being used in the FPM.

3.1. Experimental Design and Setup

The data collection for this research effort was conducted according to the improved design defined by Talafuse (2011). The experiment is described in detail below, and is very similar to the experiment on which Talafuse based his research. A few small changes were made to the original process so that more of the shots would be usable for data analysis. In designing the experiment the following five factors were considered.

1. Projectile Velocity
2. Obliquity Angle
3. Target Panel Material
4. Target Panel Thickness
5. Projectile Mass

The first four factors were tested at two different levels while projectile mass was tested at four levels. Table 3.1 shows the design points for each factor.

Table 3.1 Design Factor Values

Factor	Variable	Values	Units
Projectile Velocity	*vel*	4000	fps
		7000	
Obliquity Angle	*oblq*	0	degrees
		45	
Target Panel Material	*matrl*	AL 2024	n/a
		AL 7075	
Target Panel Thickness	*thick*	0.063	inches
		0.25	
Projectile Mass	*mass*	20	grams
		40	
		75	
		150	

A full factorial design for this test setup requires 64 shots (2×2×2×2×4 = 64). This full factorial design was preformed with five replicates for each design point. In other words, every level of every design factor was tested in combination with every level of every other design factor, and each individual configuration was tested five times. The five replicates of each design point were done to provide a more statistically significant result. This resulted in a test with 320 test shots (64×5 = 320). The designed experiment can be found in Appendix A.

The 46th Test Group, Aerospace Survivability Analysis Branch, at Wright Patterson Air Force Base conducted the preceding test in 2010. The projectiles used were steel fragments and the target panels were either 2024 or 7075 Aluminum as designated by the test design. A diagram of the test setup can be seen below in Figure 3.1. The model is not perfectly accurate, but can be used to get a good idea of what the test range looked like.

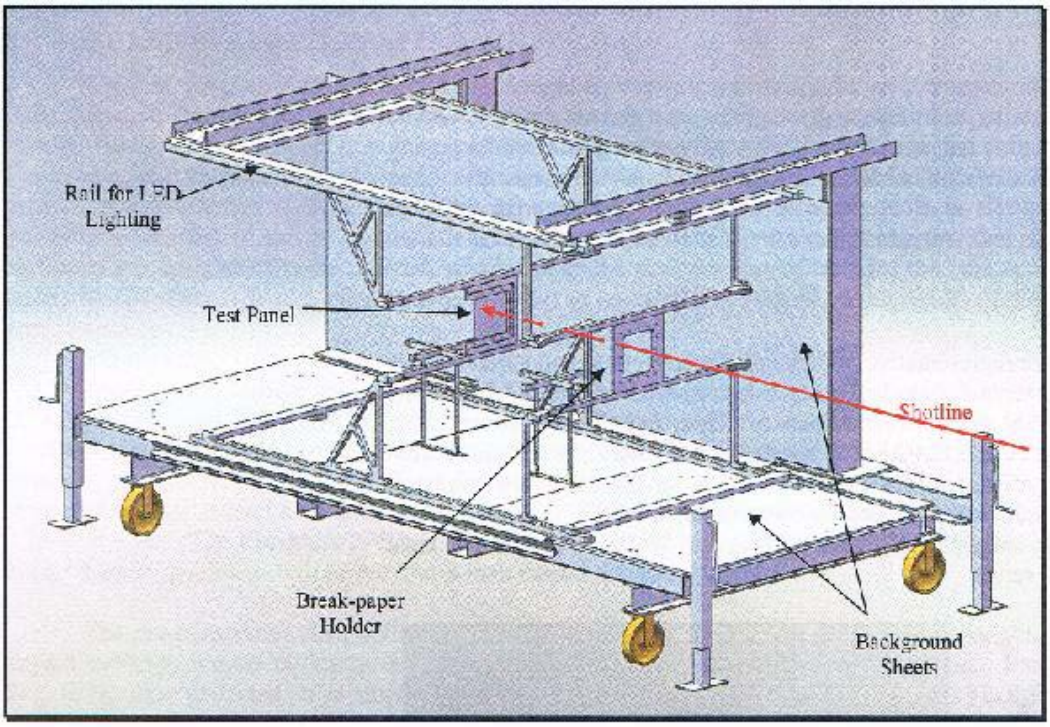

Figure 3.1 Diagram of Experimental Test Setup [10]

Break paper was used to determine the velocity of the projectile in most cases. Two sets of break paper were set up in front of the target with a known distance between them. When the projectile breaks the paper, it disrupts the electrical current running through the paper which triggers a timing device. Knowing the time the projectile took between the two break papers allows us to compute its velocity. This velocity was the value used for analysis on most of the shots. For some of the shots in the experiment the break paper did not function properly and returned no value for the velocity. In these cases, the velocity used for analysis was calculated based on the high speed video footage of the shot. This value was calculated for all shots and tended to be close to the speed calculated from the break paper.

Two high speed video cameras recorded each shot. Both cameras were placed somewhat back from the target to ensure that the entire flash was captured on film. One

of the cameras was located directly above the target panel and looking down. This camera recorded all of the shots. The second camera was located on the side of the testing apparatus. If it had been pictured in Figure 3.1, it would be on the left, looking directly at the side of the target. This second camera only recorded shots with 0 degree obliquity because the shots with 45 degree obliquity turned the plate such that the camera was not pointed directly at the side of the plate. For this reason the data obtained from the side view camera was not used in the analysis.

Most of the shots produced useable data, but some of the shots either did not produce a flash or produced a flash that was too brief to be used for the analysis. In all 283 shots out of the original 320 were used for analysis. A complete listing of the used shots grouped by their corresponding shot parameters can be found in Table 4.8.

3.2. Data Analysis

The video data obtained was analyzed using the Bestard and Kocher method, and it is assumed that the image processing data from that analysis accurately reflects the actual flash size during the test. The work done by both Henninger and Talafuse used a quartic time series model to describe the data. This approach of using a quartic model for the time series was reexamined as part of the current research effort. Figure 3.2 below shows an example of the Talafuse model compared with one of the shots from the dataset used to create that model. As can be seen from the figure, the model predicts the largest y-radius to occur just before time step 60. This shot was the only shot in the entire dataset used to create this model that has a flash radius larger than zero at time step 60. The quartic model clearly overestimates the size of the flash radius at times beyond the

average flash duration. Because of this behavior in the old model, other model types were investigated early in the analysis process.

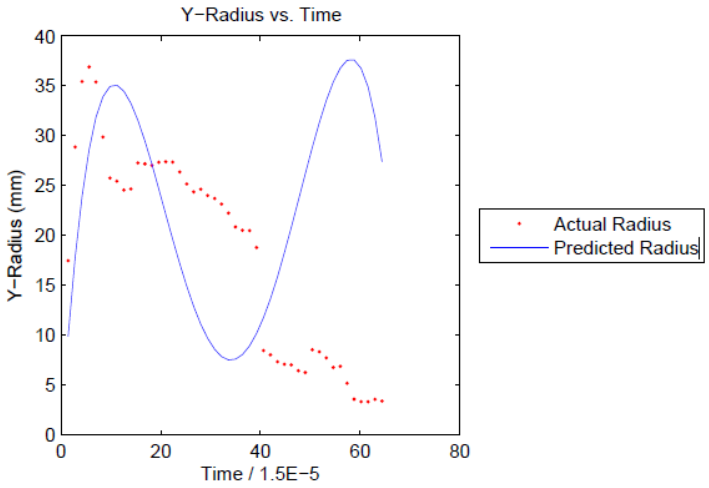

Figure 3.2 Example of Talafuse Model [10]

In the paper by Bestard and Kocher it was noted that the shape of the time series flash data closely resembled the shape of a Weibull probability distribution function (PDF). This function can take on a multitude of different shapes based on its parameters. Figure 3.3 shows several of the possible shapes of the Weibull PDF.

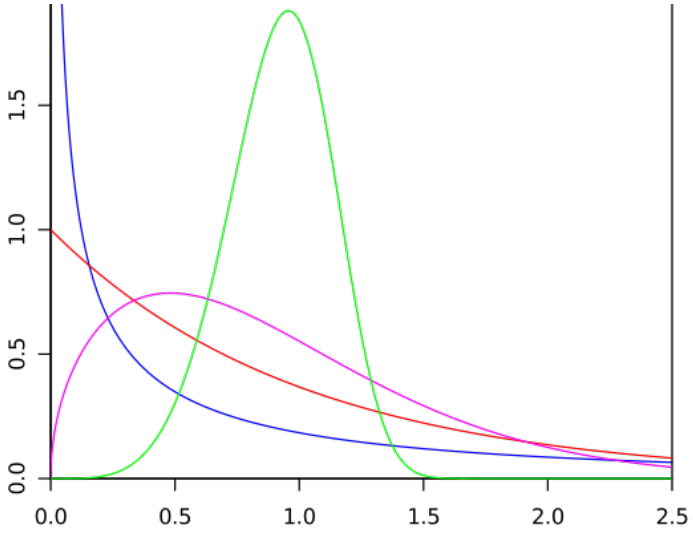

Figure 3.3 Weibull Probability Distribution Function

The Weibull PDF is not a linear function, and because of that it is slightly more complicated to estimate using least squares. However, the Weibull PDF has advantages over the quartic function when it is applied to this research. The Weibull PDF has fewer governing parameters which means that fewer data points are required for a regression using this function. In other words, more shots are available for analysis with the Weibull PDF because it can be used to analyze shots with fewer data points. Also, by setting the parameter that governs the shape of the function to one value, the Weibull PDF will more consistently create an appropriate regression of the data. Appendix B shows some comparisons of the quartic regression and a scaled Weibull PDF regression of the actual data.

Because of these advantages, the scaled Weibull PDF below was chosen as the time series model for the data.

$$Flash\ Radius(t) = \gamma\left(\left(\frac{\alpha}{\beta}\right)\left(\frac{t}{\beta}\right)^{(\alpha-1)} e^{-\left(\frac{t}{\beta}\right)^{\alpha}}\right) \tag{3.1}$$

In order to make the regression more predictable, the shape parameter (α) was set to 1.5. This results in the following equation which has only two parameters ($\beta$and γ):

$$Flash\ Radius(t) = \gamma\left(\left(\frac{1.5}{\beta}\right)\left(\frac{t}{\beta}\right)^{(1.5-1)} e^{-\left(\frac{t}{\beta}\right)^{1.5}}\right) \tag{3.2}$$

Equation 3.2 was used in the Levenburg-Marquardt algorithm to produce the least squares model. Similar to the Talafuse model, the parameters generated by this were assumed to be linearly correlated with the shot parameters in Table 3.1. As such the following meta-model was proposed for predicting the parameters of the time series model:

$$Model\ coefficient = b_0 + b_1(vel) + b_2(oblq) + b_3(matrl) + b_4(thick) + b_5(mass). \quad (3.3)$$

$b_0, b_1, \ldots, b_5$ are different unique for β and γ for both the X and Z radii of the flash. Also, $matrl$ is an indicator variable where 1 indicates that the target panel is made of 7075 Aluminum and 0 indicates that the target panel is made of 2024 Aluminum. For example, a 30 gram shard of metal impacting a panel of 7075-T651 Aluminum (which is .25 inches thick) at a velocity of 5000 fps and with zero degrees of obliquity will create a flash. The model predicts the size of the flash by first calculating the coefficients of the scaled Weibull PDF:

For the X radius:

$$\beta_x = b_0 + b_1(5000) + b_2(0) + b_3(1) + b_4(.25) + b_5(30)$$

$$\gamma_x = b_0 + b_1(5000) + b_2(0) + b_3(1) + b_4(.25) + b_5(30)$$

For the Z radius:

$$\beta_z = b_0 + b_1(5000) + b_2(0) + b_3(1) + b_4(.25) + b_5(30)$$

$$\gamma_z = b_0 + b_1(5000) + b_2(0) + b_3(1) + b_4(.25) + b_5(30)$$

Note that all four equations above have unique values for $b_0, b_1, \ldots, b_5$. The resulting four parameters are then used as the parameters of the scaled Weibull PDF so that:

$$R_x(t) = \gamma_x \left(\left(\frac{1.5}{\beta_x}\right) \left(\frac{t}{\beta_x}\right)^{(1.5-1)} e^{-\left(\frac{t}{\beta_x}\right)^{1.5}} \right) \quad (3.4)$$

$$R_z(t) = \gamma_z \left(\left(\frac{1.5}{\beta_z}\right) \left(\frac{t}{\beta_z}\right)^{(1.5-1)} e^{-\left(\frac{t}{\beta_z}\right)^{1.5}} \right) \quad (3.5)$$

Where R_x is the radius of the elliptical boundary of the flash in the X direction at time t (R_z is the radius in the Z direction). These radii define the size of an ellipse at time t. This ellipse is the predicted size of the flash at time t.

3.3. Validation Methods

In order to make sure that the model is accurate, a few forms of validation were done. The model could not be compared to any model currently in use for the prediction of a front face flash because no such model exists. As a result, cross validation was preformed to make sure that the model is adequate. The dataset used to create the model was split into two batches. Separate models were created from each batch and compared with the data from the other batch. The mean square error and of the two models was compared. As a further measure, the area under the curve of the model was compared to the area under the curve for the data. The details of the validation are addressed later in Validation section of chapter 4.

4. Results and Analysis

This chapter describes the initial analysis, the changes to the model that resulted, the following analysis of the full dataset and the final results produced. Also included are the current model equations and parameters and a presentation of the validation work done on the model.

4.1. Initial Analysis

As mentioned in section 3.3, the data was split into two batches. Upon receipt of the first batch of data, a quartic regression and a scaled Weibull PDF regression was done on the time series data for each shot. Appendix B has comparisons of the two regression models, and as discussed in chapter 3, the scaled Weibull PDF was selected as the better regression model.

Next, an initial meta-model based on equation 3.3 was created by doing a linear regression on the scaled Weibull PDF parameters. The design factors for each shot were used as the regression data while the scaled Weibull PDF regression parameters for each shot were used as the response. Using the JMP software package, the studentized residuals of the resulting meta-model were analyzed to make sure that it created a proper fit. The resulting plots for the X radius are in Figures 4.1 and 4.2 below.

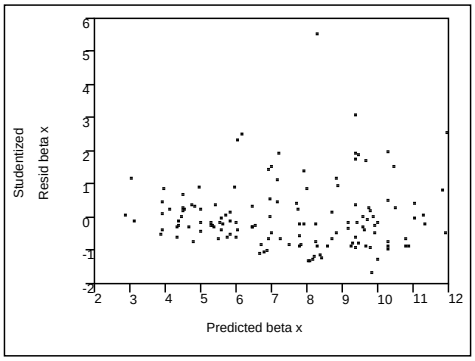

Figure 4.1 Studentized Residuals of Initial β_x Meta-Model

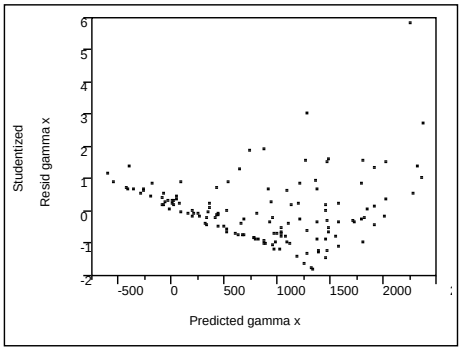

Figure 4.2 Studentized Residuals of Initial γ_x Meta-Model

Both residual plots show a fairly distinct funnel shape. As described in Montgomery, Peck and Vining, this shape indicates that a logarithmic transform of the data might improve the fit of the model [8]. As a further measure, a Box-Cox analysis was done on the model. The resulting graphs, shown in Figure 4.3, show that a logarithmic transformation might not be the optimal transformation for the data. However, the logarithmic transformation would be a better fit than the untransformed data and it is a less complicated model than the projected optimal transform.

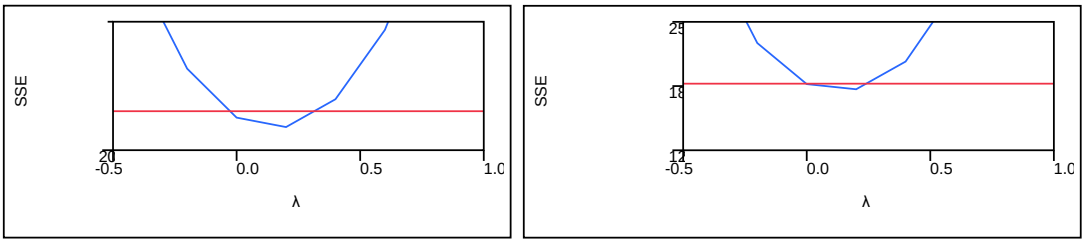

Figure 4.3 Box-Cox Analysis of β_x (left) and γ_x (right) for Initial Meta-Model

Based on this analysis a logarithmic transform of the data was taken, and the resulting meta-model was compared to the initial meta-model. The transformed model is comparatively better than the initial model. The relevant plots of the studentized residuals for this transformed model are included in Appendix C.

One further change was made to the initial meta-model equation in order to make implementation easier. Because the model is expected to expand by including new materials in the future, the $matrl$ variable was removed. Instead of the proposed indicator variable, each material has its own separate model. This change makes the model more flexible in that models for new materials will not require new indicator variables to be added to the meta-model. The above changes to the meta-model result in a couple of modifications to equation 3.3:

$$Model\ coefficient = e^{\left(b_0+b_1(vel)+b_2(oblq)+b_4(thick)+b_5(mass)\right)}. \quad (4.1)$$

This new meta-model equation was used in the data analysis that follows.

4.2. Full Dataset Analysis

Because of the changes to the meta-model, the data were separated by material. A scaled Weibull PDF regression model was made of each shot time series data. This process created a total of 283 models (141 models for AL 2024 and 142 models for AL 7075). The model parameters generated were then logarithmically transformed and a linear regression was taken of them by using the four remaining design factors as the variable data. This process created the regression coefficients of the meta-model equation (4.1). These model coefficients are seen below in Tables 4.1 and 4.2.

Table 4.1 Meta-Model Coefficients for AL 7075 Model

AL 7075 Coefficients				
Radius	X		Z	
Coefficient	β_x	γ_x	β_z	γ_z
velocity (b_1)	3.19E-05	0.000177	1.53E-05	0.000317
obliquity (b_2)	0.0118981	0.034162	0.0104189	0.036506
thickness (b_4)	0.7804977	2.303488	0.3099361	2.168843
mass (b_5)	0.0015025	0.007331	0.0012836	0.007021
intercept (b_0)	1.1058738	3.395588	1.4891721	2.508509

Table 4.2 Meta-Model Coefficients for AL 2024 Model

AL 2024 Coefficients				
Radius	X		Z	
Coefficient	β_x	γ_x	β_z	γ_z
velocity (b_1)	7.29E-06	0.000182	-4.00E-05	0.000264
obliquity (b_2)	0.0126068	0.037188	0.0113538	0.038654
thickness (b_4)	0.6632973	1.348181	0.269234	1.967688
mass (b_5)	0.0006022	0.005674	0.0004821	0.005503
intercept (b_0)	1.261354	3.531991	1.770376	2.802686

Comparing the original shot data to the model generates a fairly accurate prediction of the size of the flash radius over time. Two such comparisons are below in Figures 4.4 and 4.5.

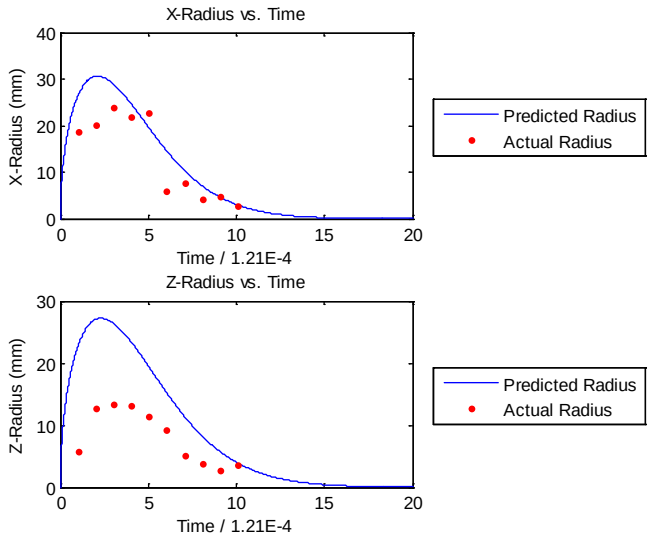

Figure 4.4 Predicted Radius Compared to Actual Radius of Shot T053

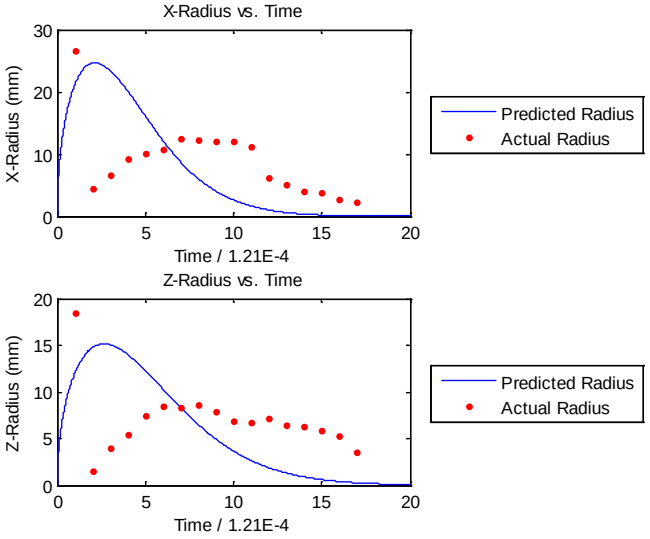

Figure 4.5 Predicted Radius Compared to Actual Radius of Shot T069

These plot show the predicted radius in comparison to the actual data. The Figure 4.4 is representative of the better comparisons between the model and the data while Figure 4.5 shows one of the not-so-good comparisons. Further analysis of the closeness of the fit between the model and the data is explored in section 4.4 on validation.

4.3. Flash Position and Orientation

Similar to the findings of Talafuse, the position of the center of the flash over time only showed recognizable trends on a shot by shot basis. Figures 4.6 and 4.7 show the X-position and Y-position versus time for the AL 2024 model. Because the data were not able to be stratified by the design factors, a simple linear regression model of the position was made:

$$Position = b_0 + b_1(Time). \tag{4.2}$$

The coefficients for the above equation are shown below in Table 4.3. Because of the randomness of the data, a stochastic model of the error could be an effective way to improve the model in the future.

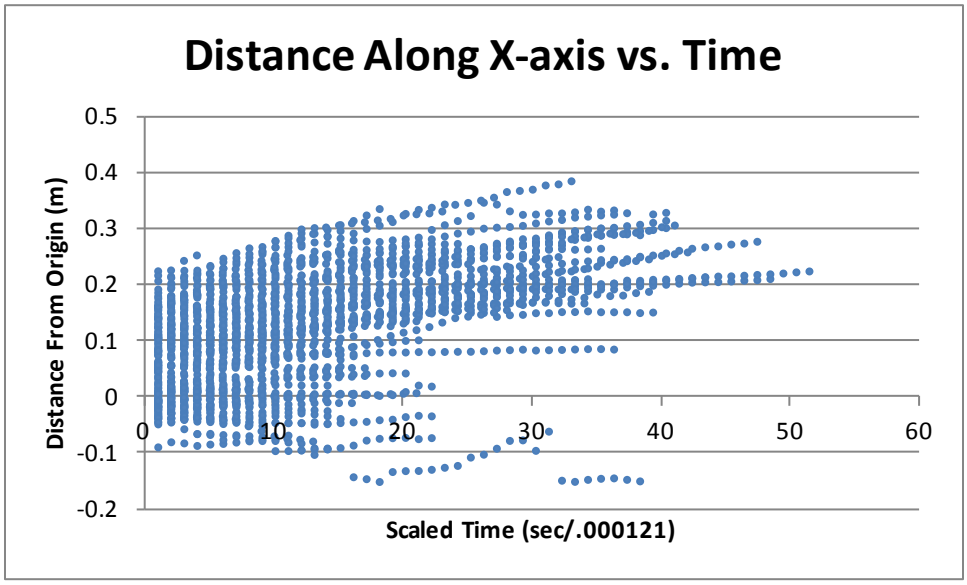

Figure 4.6 X Position vs. Time for AL 2024 Model

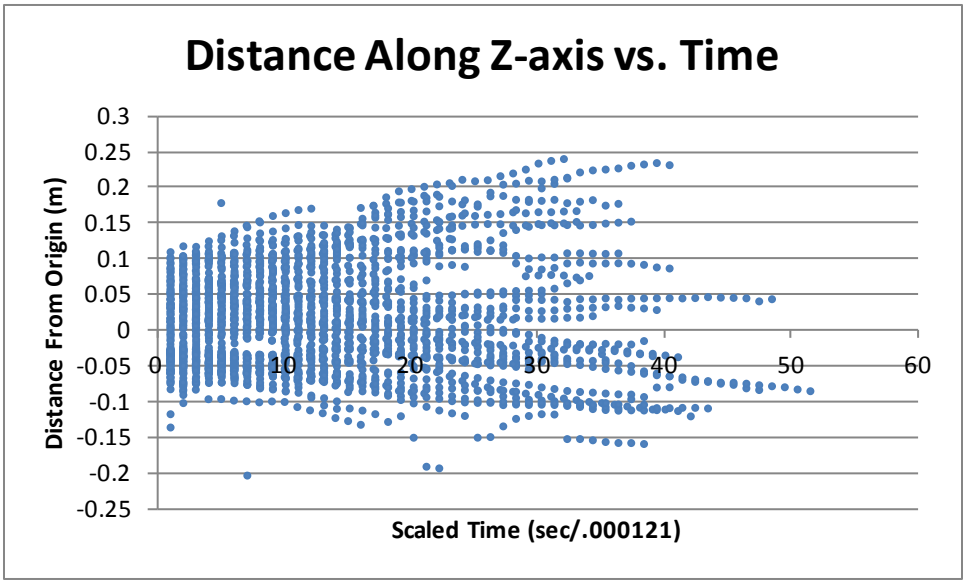

Figure 4.7 Z Position vs. Time for AL 2024 Model

Table 4.3 Position Model Coefficients

Material	Coefficient	X	Z
AL 7075	b_0	-0.07797	0.009125
	b_1	-0.00353	0.000862
AL 2024	b_0	-0.06243	0.017272
	b_1	-0.00513	0.000139

The model for the flash orientation is also similar in its approach to the Talafuse (2011) model. The flash orientation was assumed to be a random draw which is not time dependent and thus remains constant over the duration of the shot. Initial inspection shows that a normal distribution might be a good fit for the data. Figure 4.8 shows this fitted normal distribution.

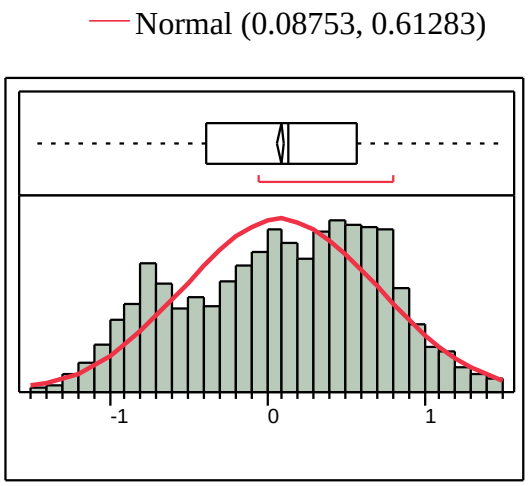

Figure 4.8 Normal Distribution Fit of Flash Orientation Data

As a further measure, the data were split into groups based on shot parameters and analyzed. The only shot parameter that appeared to have a significant effect on the shape of the distribution was the angle of obliquity. Data from shots at zero degrees of obliquity fit a normal distribution very well, but the data from shots at forty-five degrees of obliquity have a distinct bimodal tendency. Figure 4.9 shows histograms of the orientation data for both fit to normal distributions. The histogram on the left is the data from shots with zero degrees of obliquity and the one on the right is the data from shots with forty-five degrees of obliquity.

Further analysis of the orientation model was not conducted as part of this research effort, but is recommended for the future.

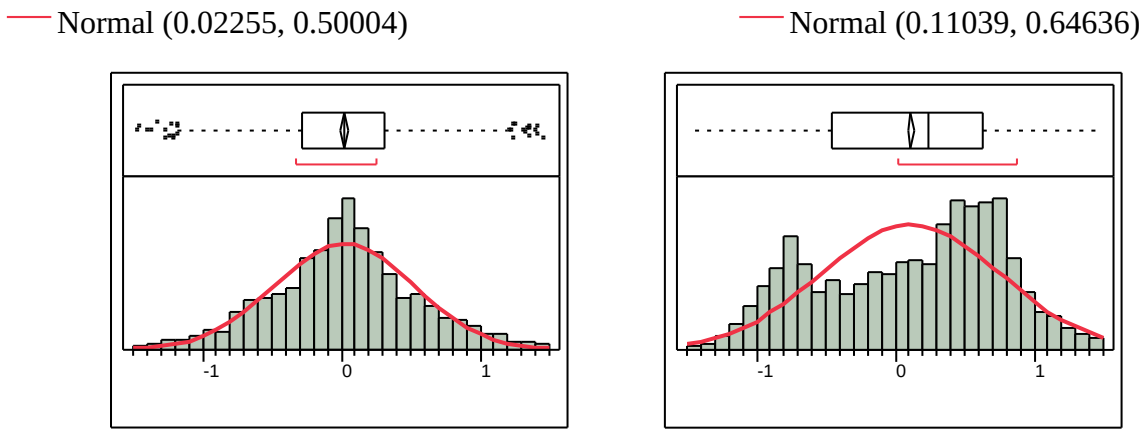

Figure 4.9 Histograms of Shot Orientation Split by Obliquity

4.4. Validation

4.4.1. Cross Validation

One of the primary concerns of the current research effort was validation. Because modeling of this type of event is largely unexplored it is important that the model be validated in any way possible. Part of this effort was using cross-validation by splitting the data into two batches (A and B). Data in the batch A were used to create a preliminary model which was compared with the data of batch B to ensure that the model could adequately predict the radius. This process was then reversed by creating a new model with batch B and comparing it back to the data from batch A. Lastly, a model of the full dataset was created and compared to the two batch models to ensure that the full model improved upon the other models. The coefficients for the batch models are shown in Tables 4.4 through 4.7.

Table 4.4 Batch A 7075 Model

Batch A 7075				
Radius	X		Z	
Coefficient	β_x	γ_x	β_z	γ_z
velocity (b_1)	1.08E-04	0.000231	9.49E-05	0.000384
obliquity (b_2)	0.008671	0.030201	0.0069033	0.031441
thickness (b_4)	1.2629592	2.338924	0.9470502	2.367032
mass (b_5)	0.0003434	0.005474	-2.57E-05	0.004997
intercept (b_0)	0.7981806	3.419211	1.1316814	2.424562

Table 4.5 Batch A 2024 Model

Batch A 2024				
Radius	X		Z	
Coefficient	β_x	γ_x	β_z	γ_z
velocity (b_1)	3.07E-05	0.000103	-2.48E-05	0.000265
obliquity (b_2)	0.0147447	0.042067	0.0146086	0.043071
thickness (b_4)	1.2888738	2.127368	0.8982552	3.038564
mass (b_5)	0.0016383	0.00662	0.0012934	0.006963
intercept (b_0)	0.8440809	3.607591	1.4255022	2.337473

Table 4.6 Batch B 7075 Model

Batch B 7075				
Radius	X		Z	
Coefficient	β_x	γ_x	β_z	γ_z
velocity (b_1)	-2.69E-05	0.000154	-4.57E-05	0.000282
obliquity (b_2)	0.0150448	0.039762	0.0136521	0.042731
thickness (b_4)	0.4525578	2.513731	-0.212193	2.164035
mass (b_5)	0.0024681	0.009465	0.0022819	0.0091
intercept (b_0)	1.3000443	3.063832	1.7467819	2.312897

Table 4.7 Batch B 2024 Model

Batch B 2024				
Radius	X		Z	
Coefficient	β_x	γ_x	β_z	γ_z
velocity (b_1)	-8.45E-06	0.000248	-5.44E-05	0.000266
obliquity (b_2)	0.0109048	0.033477	0.0085974	0.035137
thickness (b_4)	0.0313956	0.733536	-0.29972	0.970925
mass (b_5)	-0.000253	0.004677	-0.000217	0.004231
intercept (b_0)	1.6048485	3.489756	2.0766882	3.202789

The coefficients of the models appear to be reasonably similar, but cannot be compared directly without calculating confidence intervals. Appendix D has a complete listing of the shots associated with each batch as well as the details of the cross validation. The measures used for cross validation are described below in the full model validation section.

4.4.2. Full Model Validation

Two measures were used for this comparison. Because of the high amount of variability in the data and the complicated nature of the model, R^2 is not a useful statistic. Because of this the area under the curve of the predicted flash time series model was compared to the area under the curve of the time series data. This measure can be biased if the shape of the actual time series data does not match the shape of the Weibull function. In order to detect this bias the mean of the squared errors (MSE) was computed for each shot of the data using equation 4.3 below [8].

$$MSE = \frac{\sum_{i=1}^{n}(y_i - \hat{y})^2}{n - p} = \frac{SSerr}{n - p} \quad (4.3)$$

In equation 4.3 y_i is the actual radius at time step *i* based on the data, and $\hat{y}$ is the predicted radius at the same time step. *n* is the total number of data points and *p* is the number of estimators.

An unusually high MSE value on a shot that had very little difference in area would indicate that the shot data does not follow the curve of the prediction. Both of these measures were computed for each shot in the dataset. The shots were then grouped by design point and the measures for each shot in the design point were averaged. Table 4.4 shows the desired shot parameters of each design point and the shots associated with them.

Table 4.8 Design Point Descriptions

Design Point	Vel.	Obliq.	Thick.	Size	AL 7075 Shots	AL 2024 Shots
1	4000	0	0.063	20	T062,T103,T168	T137,T190
2	7000	0	0.063	20	T054,T093,T096,T142,T172	T048,T075,T116,T150,T183
3	4000	45	0.063	20	T220,T224,T284,T290,T340	T195,T247,T265,T316,T339
4	7000	45	0.063	20	T221,T225,T271,T297,T343	T204,T229,T282,T298,T330
5	4000	0	0.25	20	T059,T088,T144	T052,T076,T100,T129,T182
6	7000	0	0.25	20	T036,T064,T121,T129,T165	T053,T084,T117,T143,T159
7	4000	45	0.25	20	T218,T243,T278,T308,T334	T199,T246,T255,T294,T320
8	7000	45	0.25	20	T219,T251,T269,T291,T319	T192,T226,T266,T305,T323
9	4000	0	0.063	40	T061,T06,T101,T167	T083,T099,T138,T164
10	7000	0	0.063	40	T037,T068,T107,T160	T057,T080,T098,T152,T163
11	4000	45	0.063	40	T205,T231,T268,T304,T321	T207,T230,T261,T288,T322
12	7000	45	0.063	40	T191,T250,T285,T318,T332	T215,T241,T263,T309,T324
13	4000	0	0.25	40	T042,T079,T102,T131,T161	T056,T065,T180
14	7000	0	0.25	40	T034,T072,T105,T141,T178	T058,T091,T112,T133,T166
15	4000	45	0.25	40	T200,T237,T256,T317,T336	T244,T270,T296,T328
16	7000	45	0.25	40	T214,T242,T260,T300,T345	T222,T233,T259,T299,T327
17	4000	0	0.063	75	T039,T082,T124,T170	none
18	7000	0	0.063	75	T032,T090,T097,T145,T181	T049,T070,T123,T130

Design Point	Vel.	Obliq.	Thick.	Size	AL 7075 Shots	AL 2024 Shots
19	4000	45	0.063	75	T208,T240,T275,T307,T338	T210,T253,T257,T312,T348
20	7000	45	0.063	75	T197,T232,T279,T293,T326	T201,T227,T267,T311,T329
21	4000	0	0.25	75	T031	T035,T069,T173
22	7000	0	0.25	75	T089,T119,T158	T047,T085,T106,T134,T186
23	4000	45	0.25	75	T209,T239,T280,T314,T341	T193,T252,T258,T292,T347
24	7000	45	0.25	75	T211,T254,T283,T310,T346	T206,T238,T277,T301,T331
25	4000	0	0.063	150	T051,T120,T184	T038,T071,T108
26	7000	0	0.063	150	T046,T081,T114,T128,T177	T040,T074,T122,T169
27	4000	45	0.063	150	T203,T248,T264,T315,T350	T217,T234,T274,T289,T333
28	7000	45	0.063	150	T198,T223,T281,T303,T337	T213,T228,T273,T302,T349
29	4000	0	0.25	150	T043,T078	T044,T092,T104,T147
30	7000	0	0.25	150	T033,T063,T111,T151,T185	T045,T094,T125,T156,T189
31	4000	45	0.25	150	T194,Y249,T272,T287,T342	T202,T235,T286,T295,T344
32	7000	45	0.25	150	T212,T245,T276,T313,T325	T196,T236,T262,T306,T335

As mentioned in the Methodology chapter, all of the design points originally had five test shots. Due to a lack of usable data for some of the test shots, some of the design points have less than five shots worth of data. All design points except for 21 and 17 have multiple shots associated with them for each model. Design point 21 only has one shot for the 7075 Model and as such the average area value calculated next depends only on this one shot. Similarly, design point 17 has zero shots with data in the 2024 model and therefore does not have an area calculation.

Figure 4.10 is one of the resulting bar graphs which compares the area under the curve of the predicted radius compared to the area under the curve of the actual flash data. The graphs for all of the full models are included in Appendix E, however the other graphs show similar results to those shown in Figure 4.10.

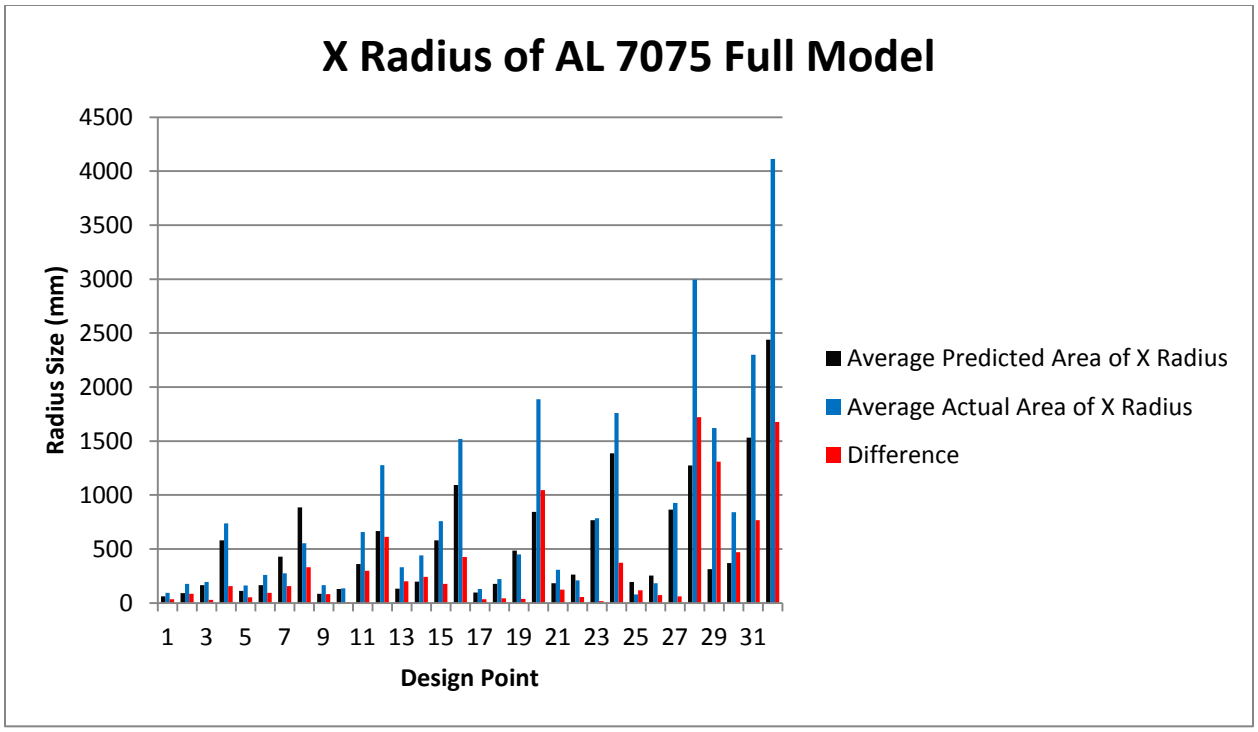

Figure 4.10 Comparison of Area Under the Curve for X-Radius of AL 7075 Model

In this case, the difference between the actual radius and the predicted radius is larger than the actual flash for one of the design points (25), but for many of the others this difference is very small. As stated above, these small values could be biased, so to help analyze this possibility the MSE values are analyzed. Figure 4.11 shows the MSE values for the AL 7075 model.

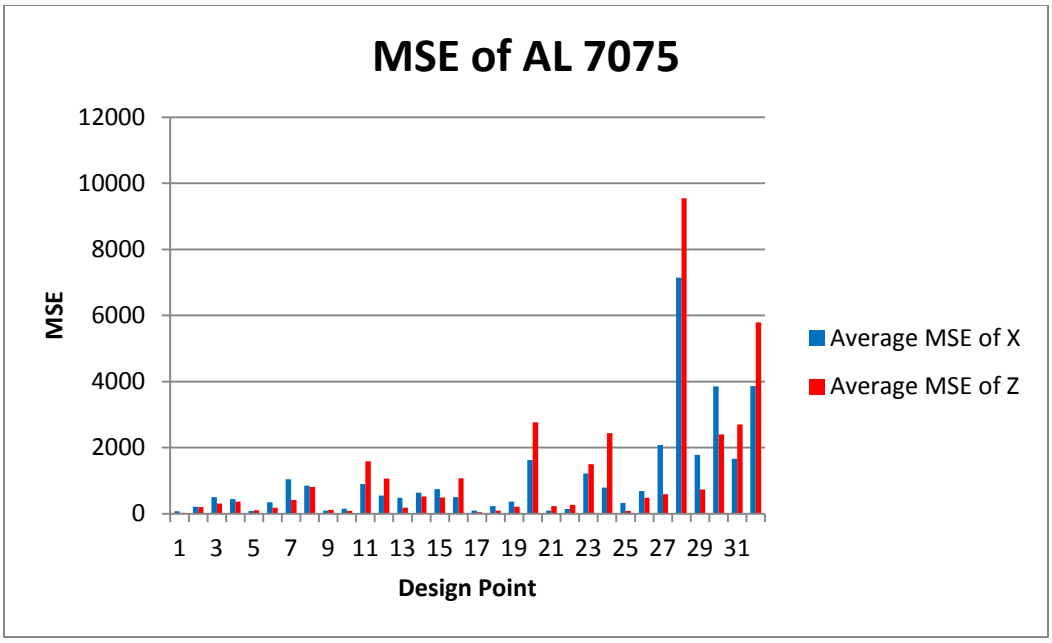

Figure 4.11 MSE Comparison for AL 7075 Model

The design points with high MSE values tend to be the same ones with large differences in the area comparison. As such, this analysis does not indicate any significant bias in the area comparison.

Lastly, the difference between the model and data was calculated as a percent difference from the actual flash size. Results of this analysis are shown in Tables 4.5 and 4.6.

Table 4.9 AL 7075 Validation Table

Design Point	Average MSE_x	Percentage Area Difference X	Average MSE_z	Percentage Area Difference Z
1	75.18098	35%	20.88594	27%
2	203.8393	48%	202.0421	48%
3	497.4702	15%	304.0814	56%
4	443.5636	21%	364.4563	26%
5	79.23281	32%	103.5714	53%
6	341.8219	36%	184.2077	15%
7	1039.557	57%	407.5636	73%
8	843.8121	60%	808.7659	50%

Design Point	Average MSE_x	Percentage Area Difference X	Average MSE_z	Percentage Area Difference Z
9	96.07515	49%	113.8182	61%
10	149.2157	4%	84.74783	16%
11	895.1966	45%	1587.156	71%
12	551.9976	48%	1057.685	54%
13	475.3991	60%	183.1734	64%
14	634.2422	55%	517.4325	52%
15	738.4809	23%	488.6838	17%
16	497.9644	28%	1073.803	33%
17	88.22129	26%	46.08351	37%
18	225.8667	20%	95.99259	22%
19	362.5555	8%	210.6621	53%
20	1619.621	55%	2769.268	59%
21	91.19154	41%	232.101	62%
22	140.646	26%	267.6073	1%
23	1215.059	2%	1494.947	34%
24	788.5343	21%	2434.264	33%
25	320.6481	148%	86.8982	105%
26	680.5239	40%	484.1553	54%
27	2081.811	7%	584.7686	1%
28	7144.453	57%	9542.17	62%
29	1779.696	81%	736.086	81%
30	3846.305	56%	2397.342	50%
31	1657.754	33%	2701.918	37%
32	3860.635	41%	5788.227	43%

Table 4.10 AL 2024 Validation Table

Design Point	Average MSE_x	Percentage Area Difference X	Average MSE_z	Percentage Area Difference Z
1	1378.409	47%	145.5494	36%
2	497.9136	49%	208.4037	55%
3	258.5047	40%	81.18905	20%
4	795.2859	36%	308.1212	22%
5	549.9913	8%	462.3149	3%
6	75.60483	12%	121.9858	1%
7	2562.119	45%	1212.024	48%
8	1526.652	24%	1078.761	30%
9	1411.913	49%	415.1763	33%
10	920.4365	28%	2056.286	43%
11	853.6359	37%	589.9256	57%
12	618.6434	24%	3876.663	48%

Design Point	Average MSE_x	Percentage Area Difference X	Average MSE_z	Percentage Area Difference Z
13	1430.036	16%	323.4347	28%
14	5438.711	51%	1741.705	35%
15	954.0566	30%	301.6687	4%
16	185.25	49%	146.9257	47%
17	-	-	-	-
18	231.9815	51%	320.1733	68%
19	627.8537	2%	434.8686	21%
20	735.3856	68%	980.0249	76%
21	349.8684	27%	238.5319	20%
22	324.2354	40%	227.9718	30%
23	719.6601	54%	383.9309	45%
24	2175.431	47%	5341.563	62%
25	1259.018	38%	5151.802	59%
26	4045.788	54%	2254.798	46%
27	2586.016	42%	1147.176	28%
28	755.5244	30%	1558.047	40%
29	1147.385	10%	895.9965	19%
30	655.7699	2%	486.4299	35%
31	1104.242	24%	963.3159	47%
32	2040.664	42%	968.1821	42%

The above tables show the results of the validation in a slightly different light. This representation of the validation shows that the area calculation for some of the design points may have a fair amount of bias. Points in which the area calculation could have a high degree of bias are 23 and 27 in the AL 7075 model and point 30 in the AL 2024 model. Other than these points the area calculation appears to be a relatively good measure for comparison.

5. Conclusions, Recommendations, and Future Work

The current research effort into the flash created by incoming steel fragments on aluminum targets has produced some interesting results and a new prediction model. Over the course of this research effort the proposed model went through several iterations. The original idea of using a quartic regression model to predict the radius of the flash was abandoned in favor of a scaled Weibull PDF regression model. The meta-model was changed from a regular linear regression using all five of the design parameters to a logarithmically transformed linear regression where each material has its own separate model. The resulting model creates a reasonably accurate prediction of a flash event using the parameters of the shot. This model was then validated and found to be adequate. The model described was delivered and at the time of this report is being implemented into the joint survivability modeling toolbox.

In conclusion, based on the results of this research effort and the validation that was performed on those results, the model developed has been implemented into the FPM. Despite some questionable amount of validity, it improves upon the FPM because it predicts the size and duration of the front face flash created from an incoming, non-incendiary fragment with some degree of accuracy.

Future work on and development of this model is recommended. Several things can be done to make this model more efficient and more effective for predicting ballistic impact flashes. One small but helpful change would be changing the units of the incoming design parameters to metric. Currently the input parameters are in United States customary units while the outputs of the model are in the metric system. Another

item requiring some future work is the investigation of the bimodality of the flash orientation.

Two other areas of future work could expand and greatly improve the usefulness of the model. Development of a stochastic model of the error term in model would make model predictions more realistic, and could lead to a more in depth understanding of the flash process in general. This stochastic model would give aircraft designers more information so they could make more aggressive decisions with more confidence. One last area of future work is the expansion of the model to include new materials. Composite materials in particular would be a good place to expand the current model because they are used often in the design of new aircraft. A more ambitious way to implement this would be to attempt to add coefficients for material properties (e.g. tensile strength or Young's modulus) to the meta-model. Pursuit of any of these opportunities for future should improve upon the current research effort and thereby further the overall goal of producing a better aircraft.

Appendix A: Designed Experiment Details

Test No.	Velocity (fps)	Obliquity (deg)	Material Type	Thickness (in)	Frag Size (grain)
T031	4000	0	7075 T651	0.25	75
T032	7000	0	7075 T6	0.063	75
T033	7000	0	7075 T651	0.25	150
T034	7000	0	7075 T651	0.25	40
T035	4000	0	2024 T351	0.25	75
T036	7000	0	7075 T651	0.25	20
T037	7000	0	7075 T6	0.063	40
T038	4000	0	2024 T3	0.063	150
T039	4000	0	7075 T6	0.063	75
T040	7000	0	2024 T3	0.063	150
T041	4000	0	2024 T3	0.063	20
T042	4000	0	7075 T651	0.25	40
T043	4000	0	7075 T651	0.25	150
T044	4000	0	2024 T351	0.25	150
T045	7000	0	2024 T351	0.25	150
T046	7000	0	7075 T6	0.063	150
T047	7000	0	2024 T351	0.25	75
T048	7000	0	2024 T3	0.063	20
T049	7000	0	2024 T3	0.063	75
T050	4000	0	2024 T3	0.063	75
T051	4000	0	7075 T6	0.063	150
T052	4000	0	2024 T351	0.25	20
T053	7000	0	2024 T351	0.25	20
T054	7000	0	7075 T6	0.063	20
T055	7000	0	7075 T651	0.25	75
T056	4000	0	2024 T351	0.25	40
T057	7000	0	2024 T3	0.063	40
T058	7000	0	2024 T351	0.25	40
T059	4000	0	7075 T651	0.25	20
T060	4000	0	2024 T3	0.063	40
T061	4000	0	7075 T6	0.063	40
T062	4000	0	7075 T6	0.063	20
T063	7000	0	7075 T651	0.25	150
T064	7000	0	7075 T651	0.25	20
T065	4000	0	2024 T351	0.25	40
T066	4000	0	7075 T6	0.063	40
T067	4000	0	7075 T651	0.25	75

Test No.	Velocity	Obliquity	Material Type	Thickness	Frag Size
T068	7000	0	7075 T6	0.063	40
T069	4000	0	2024 T351	0.25	75
T070	7000	0	2024 T3	0.063	75
T071	4000	0	2024 T3	0.063	150
T072	7000	0	7075 T651	0.25	40
T073	4000	0	2024 T3	0.063	20
T074	7000	0	2024 T3	0.063	150
T075	7000	0	2024 T3	0.063	20
T076	4000	0	2024 T351	0.25	20
T077	4000	0	7075 T6	0.063	150
T078	4000	0	7075 T651	0.25	150
T079	4000	0	7075 T651	0.25	40
T080	7000	0	2024 T3	0.063	40
T081	7000	0	7075 T6	0.063	150
T082	4000	0	7075 T6	0.063	75
T083	4000	0	2024 T3	0.063	40
T084	7000	0	2024 T351	0.25	20
T085	7000	0	2024 T351	0.25	75
T086	4000	0	7075 T6	0.063	20
T087	4000	0	2024 T3	0.063	75
T088	4000	0	7075 T651	0.25	20
T089	7000	0	7075 T651	0.25	75
T090	7000	0	7075 T6	0.063	75
T091	7000	0	2024 T351	0.25	40
T092	4000	0	2024 T351	0.25	150
T093	7000	0	7075 T6	0.063	20
T094	7000	0	2024 T351	0.25	150
T095	4000	0	2024 T3	0.063	75
T096	7000	0	7075 T6	0.063	20
T097	7000	0	7075 T6	0.063	75
T098	7000	0	2024 T3	0.063	40
T099	4000	0	2024 T3	0.063	40
T100	4000	0	2024 T351	0.25	20
T101	4000	0	7075 T6	0.063	40
T102	4000	0	7075 T651	0.25	40
T103	4000	0	7075 T6	0.063	20
T104	4000	0	2024 T351	0.25	150
T105	7000	0	7075 T651	0.25	40
T106	7000	0	2024 T351	0.25	75
T107	7000	0	7075 T6	0.063	40

Test No.	Velocity	Obliquity	Material Type	Thickness	Frag Size
T108	4000	0	2024 T3	0.063	150
T109	4000	0	7075 T651	0.25	150
T110	4000	0	2024 T351	0.25	40
T111	7000	0	7075 T651	0.25	150
T112	7000	0	2024 T351	0.25	40
T113	4000	0	7075 T651	0.25	75
T114	7000	0	7075 T6	0.063	150
T115	4000	0	2024 T3	0.063	20
T116	7000	0	2024 T3	0.063	20
T117	7000	0	2024 T351	0.25	20
T118	4000	0	7075 T651	0.25	20
T119	7000	0	7075 T651	0.25	75
T120	4000	0	7075 T6	0.063	150
T121	7000	0	7075 T651	0.25	20
T122	7000	0	2024 T3	0.063	150
T123	7000	0	2024 T3	0.063	75
T124	4000	0	7075 T6	0.063	75
T125	7000	0	2024 T351	0.25	150
T126	4000	0	2024 T351	0.25	75
T127	4000	0	2024 T351	0.25	20
T128	7000	0	7075 T6	0.063	150
T129	7000	0	7075 T651	0.25	20
T130	7000	0	2024 T3	0.063	75
T131	4000	0	7075 T651	0.25	40
T132	4000	0	7075 T6	0.063	20
T133	7000	0	2024 T351	0.25	40
T134	7000	0	2024 T351	0.25	75
T135	4000	0	2024 T351	0.25	75
T136	4000	0	2024 T3	0.063	150
T137	4000	0	2024 T3	0.063	20
T138	4000	0	2024 T3	0.063	40
T139	4000	0	7075 T6	0.063	75
T140	4000	0	7075 T6	0.063	150
T141	7000	0	7075 T651	0.25	40
T142	7000	0	7075 T6	0.063	20
T143	7000	0	2024 T351	0.25	20
T144	4000	0	7075 T651	0.25	20
T145	7000	0	7075 T6	0.063	75
T146	7000	0	2024 T3	0.063	150
T147	4000	0	2024 T351	0.25	150

Test No.	Velocity	Obliquity	Material Type	Thickness	Frag Size
T148	7000	0	7075 T6	0.063	40
T149	4000	0	7075 T651	0.25	150
T150	7000	0	2024 T3	0.063	20
T151	7000	0	7075 T651	0.25	150
T152	7000	0	2024 T3	0.063	40
T153	4000	0	7075 T6	0.063	40
T154	4000	0	7075 T651	0.25	75
T155	4000	0	2024 T3	0.063	75
T156	7000	0	2024 T351	0.25	150
T157	4000	0	2024 T351	0.25	40
T158	7000	0	7075 T651	0.25	75
T159	7000	0	2024 T351	0.25	20
T160	7000	0	7075 T6	0.063	40
T161	4000	0	7075 T651	0.25	40
T162	7000	0	2024 T3	0.063	75
T163	7000	0	2024 T3	0.063	40
T164	4000	0	2024 T3	0.063	40
T165	7000	0	7075 T651	0.25	20
T166	7000	0	2024 T351	0.25	40
T167	4000	0	7075 T6	0.063	40
T168	4000	0	7075 T6	0.063	20
T169	7000	0	2024 T3	0.063	150
T170	4000	0	7075 T6	0.063	75
T171	4000	0	2024 T3	0.063	40
T172	7000	0	7075 T6	0.063	20
T173	4000	0	2024 T351	0.25	75
T174	4000	0	2024 T351	0.25	150
T175	7000	0	7075 T651	0.25	75
T176	4000	0	7075 T651	0.25	75
T177	7000	0	7075 T6	0.063	150
T178	7000	0	7075 T651	0.25	40
T179	4000	0	2024 T3	0.063	150
T180	4000	0	2024 T351	0.25	40
T181	7000	0	7075 T6	0.063	75
T182	4000	0	2024 T351	0.25	20
T183	7000	0	2024 T3	0.063	20
T184	4000	0	7075 T6	0.063	150
T185	7000	0	7075 T651	0.25	150
T186	7000	0	2024 T351	0.25	75
T187	4000	0	7075 T651	0.25	20

Test No.	Velocity	Obliquity	Material Type	Thickness	Frag Size
T188	4000	0	7075 T651	0.25	150
T189	7000	0	2024 T351	0.25	150
T190	4000	0	2024 T3	0.063	20
T191	7000	45	7075 T6	0.063	40
T192	7000	45	2024 T351	0.25	20
T193	4000	45	2024 T351	0.25	75
T194	4000	45	7075 T651	0.25	150
T195	4000	45	2024 T3	0.063	20
T196	7000	45	2024 T351	0.25	150
T197	7000	45	7075 T6	0.063	75
T198	7000	45	7075 T6	0.063	150
T199	4000	45	2024 T351	0.25	20
T200	4000	45	7075 T651	0.25	40
T201	7000	45	2024 T3	0.063	75
T202	4000	45	2024 T351	0.25	150
T203	4000	45	7075 T6	0.063	150
T204	7000	45	2024 T3	0.063	20
T205	4000	45	7075 T6	0.063	40
T206	7000	45	2024 T351	0.25	75
T207	4000	45	2024 T3	0.063	40
T208	4000	45	7075 T6	0.063	75
T209	4000	45	7075 T651	0.25	75
T210	4000	45	2024 T3	0.063	75
T211	7000	45	7075 T651	0.25	75
T212	7000	45	7075 T651	0.25	150
T213	7000	45	2024 T3	0.063	150
T214	7000	45	7075 T651	0.25	40
T215	7000	45	2024 T3	0.063	40
T216	4000	45	2024 T351	0.25	40
T217	4000	45	2024 T3	0.063	150
T218	4000	45	7075 T651	0.25	20
T219	7000	45	7075 T651	0.25	20
T220	4000	45	7075 T6	0.063	20
T221	7000	45	7075 T6	0.063	20
T222	7000	45	2024 T351	0.25	40
T223	7000	45	7075 T6	0.063	150
T224	4000	45	7075 T6	0.063	20
T225	7000	45	7075 T6	0.063	20
T226	7000	45	2024 T351	0.25	20
T227	7000	45	2024 T3	0.063	75

Test No.	Velocity	Obliquity	Material Type	Thickness	Frag Size
T228	7000	45	2024 T3	0.063	150
T229	7000	45	2024 T3	0.063	20
T230	4000	45	2024 T3	0.063	40
T231	4000	45	7075 T6	0.063	40
T232	7000	45	7075 T6	0.063	75
T233	7000	45	2024 T351	0.25	40
T234	4000	45	2024 T3	0.063	150
T235	4000	45	2024 T351	0.25	150
T236	7000	45	2024 T351	0.25	150
T237	4000	45	7075 T651	0.25	40
T238	7000	45	2024 T351	0.25	75
T239	4000	45	7075 T651	0.25	75
T240	4000	45	7075 T6	0.063	75
T241	7000	45	2024 T3	0.063	40
T242	7000	45	7075 T651	0.25	40
T243	4000	45	7075 T651	0.25	20
T244	4000	45	2024 T351	0.25	40
T245	7000	45	7075 T651	0.25	150
T246	4000	45	2024 T351	0.25	20
T247	4000	45	2024 T3	0.063	20
T248	4000	45	7075 T6	0.063	150
T249	4000	45	7075 T651	0.25	150
T250	7000	45	7075 T6	0.063	40
T251	7000	45	7075 T651	0.25	20
T252	4000	45	2024 T351	0.25	75
T253	4000	45	2024 T3	0.063	75
T254	7000	45	7075 T651	0.25	75
T255	4000	45	2024 T351	0.25	20
T256	4000	45	7075 T651	0.25	40
T257	4000	45	2024 T3	0.063	75
T258	4000	45	2024 T351	0.25	75
T259	7000	45	2024 T351	0.25	40
T260	7000	45	7075 T651	0.25	40
T261	4000	45	2024 T3	0.063	40
T262	7000	45	2024 T351	0.25	150
T263	7000	45	2024 T3	0.063	40
T264	4000	45	7075 T6	0.063	150
T265	4000	45	2024 T3	0.063	20
T266	7000	45	2024 T351	0.25	20
T267	7000	45	2024 T3	0.063	75

Test No.	Velocity	Obliquity	Material Type	Thickness	Frag Size
T268	4000	45	7075 T6	0.063	40
T269	7000	45	7075 T651	0.25	20
T270	4000	45	2024 T351	0.25	40
T271	7000	45	7075 T6	0.063	20
T272	4000	45	7075 T651	0.25	150
T273	7000	45	2024 T3	0.063	150
T274	4000	45	2024 T3	0.063	150
T275	4000	45	7075 T6	0.063	75
T276	7000	45	7075 T651	0.25	150
T277	7000	45	2024 T351	0.25	75
T278	4000	45	7075 T651	0.25	20
T279	7000	45	7075 T6	0.063	75
T280	4000	45	7075 T651	0.25	75
T281	7000	45	7075 T6	0.063	150
T282	7000	45	2024 T3	0.063	20
T283	7000	45	7075 T651	0.25	75
T284	4000	45	7075 T6	0.063	20
T285	7000	45	7075 T6	0.063	40
T286	4000	45	2024 T351	0.25	150
T287	4000	45	7075 T651	0.25	150
T288	4000	45	2024 T3	0.063	40
T289	4000	45	2024 T3	0.063	150
T290	4000	45	7075 T6	0.063	20
T291	7000	45	7075 T651	0.25	20
T292	4000	45	2024 T351	0.25	75
T293	7000	45	7075 T6	0.063	75
T294	4000	45	2024 T351	0.25	20
T295	4000	45	2024 T351	0.25	150
T296	4000	45	2024 T351	0.25	40
T297	7000	45	7075 T6	0.063	20
T298	7000	45	2024 T3	0.063	20
T299	7000	45	2024 T351	0.25	40
T300	7000	45	7075 T651	0.25	40
T301	7000	45	2024 T351	0.25	75
T302	7000	45	2024 T3	0.063	150
T303	7000	45	7075 T6	0.063	150
T304	4000	45	7075 T6	0.063	40
T305	7000	45	2024 T351	0.25	20
T306	7000	45	2024 T351	0.25	150
T307	4000	45	7075 T6	0.063	75

Test No.	Velocity	Obliquity	Material Type	Thickness	Frag Size
T308	4000	45	7075 T651	0.25	20
T309	7000	45	2024 T3	0.063	40
T310	7000	45	7075 T651	0.25	75
T311	7000	45	2024 T3	0.063	75
T312	4000	45	2024 T3	0.063	75
T313	7000	45	7075 T651	0.25	150
T314	4000	45	7075 T651	0.25	75
T315	4000	45	7075 T6	0.063	150
T316	4000	45	2024 T3	0.063	20
T317	4000	45	7075 T651	0.25	40
T318	7000	45	7075 T6	0.063	40
T319	7000	45	7075 T651	0.25	20
T320	4000	45	2024 T351	0.25	20
T321	4000	45	7075 T6	0.063	40
T322	4000	45	2024 T3	0.063	40
T323	7000	45	2024 T351	0.25	20
T324	7000	45	2024 T3	0.063	40
T325	7000	45	7075 T651	0.25	150
T326	7000	45	7075 T6	0.063	75
T327	7000	45	2024 T351	0.25	40
T328	4000	45	2024 T351	0.25	40
T329	7000	45	2024 T3	0.063	75
T330	7000	45	2024 T3	0.063	20
T331	7000	45	2024 T351	0.25	75
T332	7000	45	7075 T6	0.063	40
T333	4000	45	2024 T3	0.063	150
T334	4000	45	7075 T651	0.25	20
T335	7000	45	2024 T351	0.25	150
T336	4000	45	7075 T651	0.25	40
T337	7000	45	7075 T6	0.063	150
T338	4000	45	7075 T6	0.063	75
T339	4000	45	2024 T3	0.063	20
T340	4000	45	7075 T6	0.063	20
T341	4000	45	7075 T651	0.25	75
T342	4000	45	7075 T651	0.25	150
T343	7000	45	7075 T6	0.063	20
T344	4000	45	2024 T351	0.25	150
T345	7000	45	7075 T651	0.25	40
T346	7000	45	7075 T651	0.25	75
T347	4000	45	2024 T351	0.25	75

Test No.	Velocity	Obliquity	Material Type	Thickness	Frag Size
T348	4000	45	2024 T3	0.063	75
T349	7000	45	2024 T3	0.063	150
T350	4000	45	7075 T6	0.063	150

Appendix B: Comparisons of Weibull and Quartic Regressions

T097 Quartic

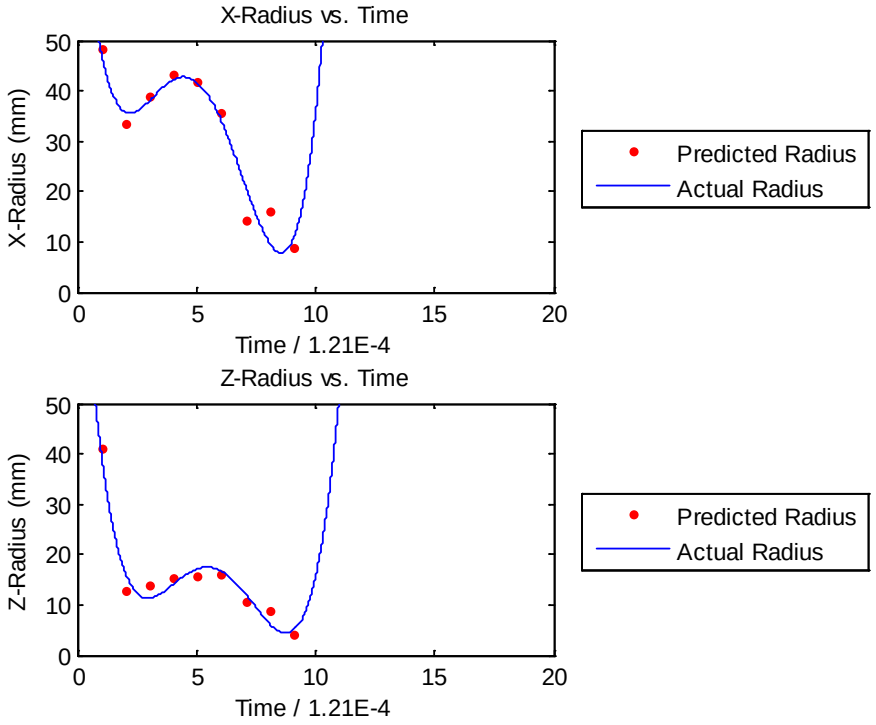

T097 Weibull

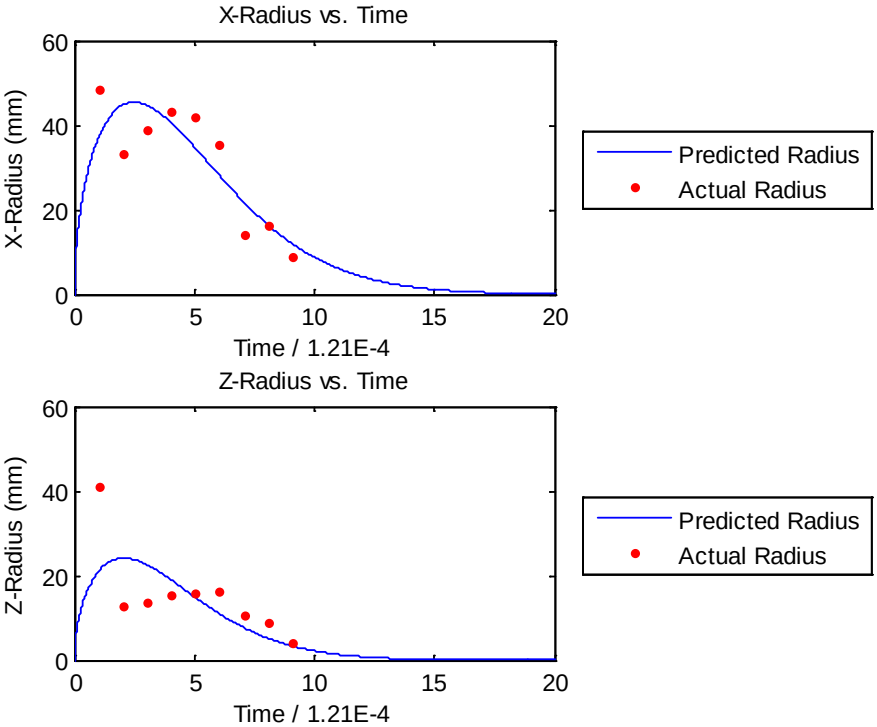

T127 Quartic

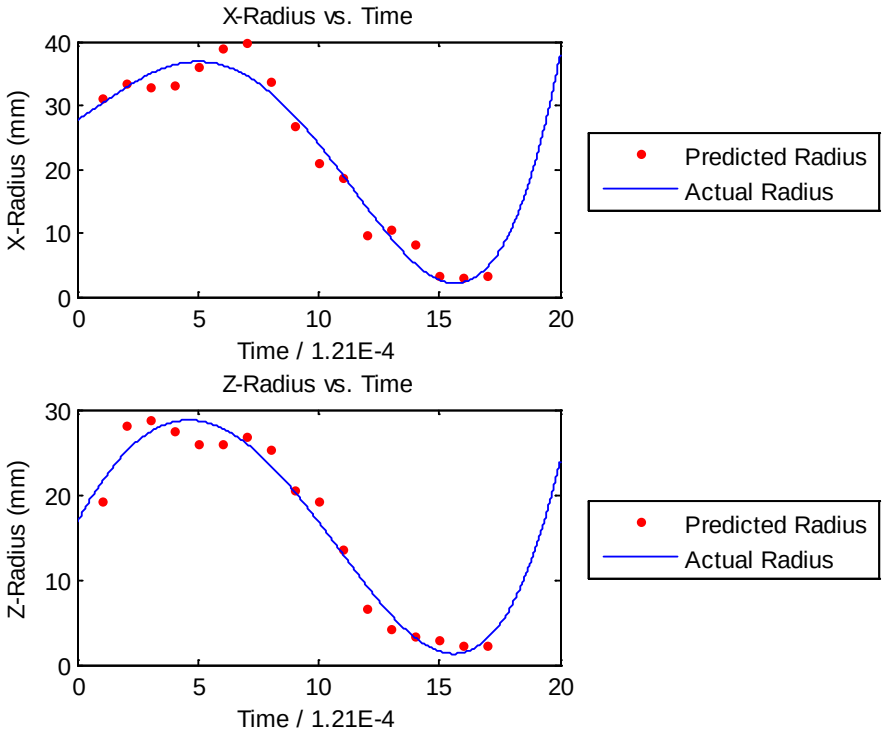

T127 Weibull

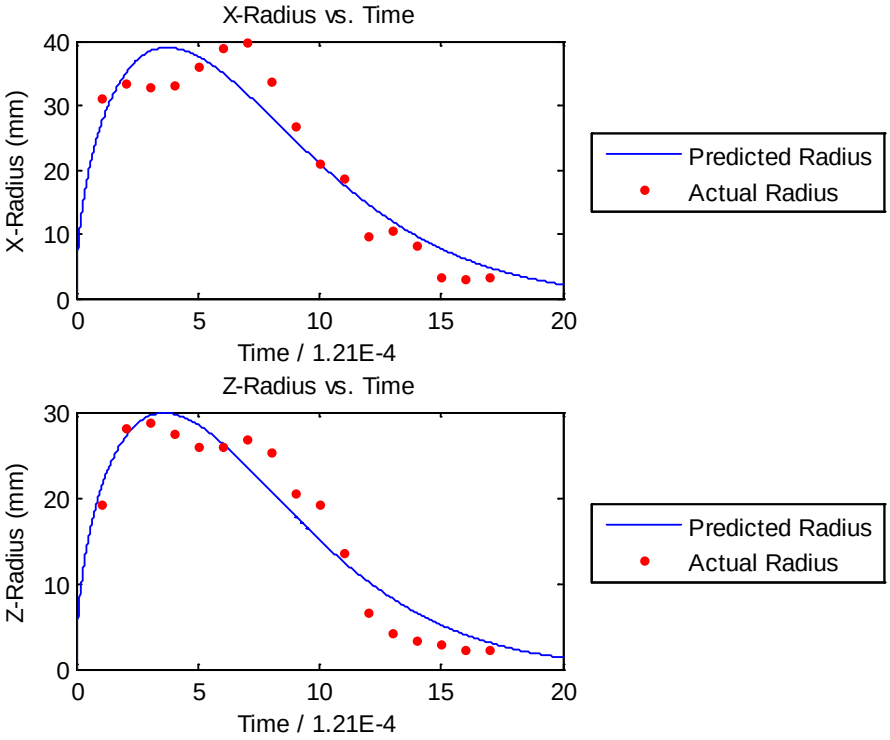

Appendix C: Residual Analysis of Meta-Model

Transformed Meta-Model Residuals

β_x

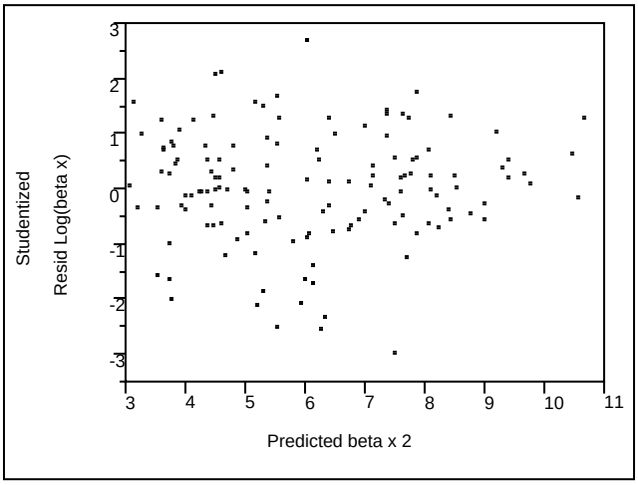

γ_x

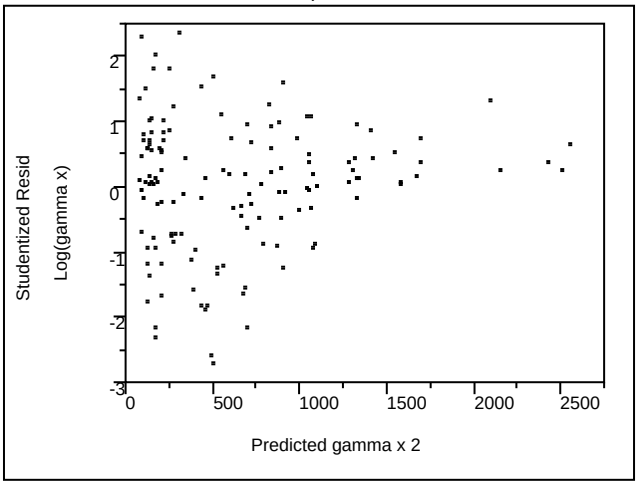

β_z

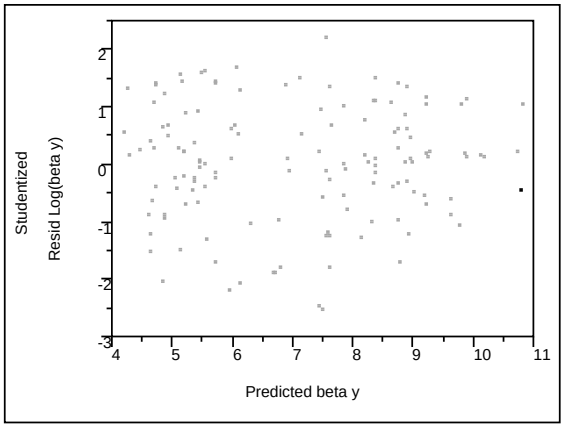

γ_z

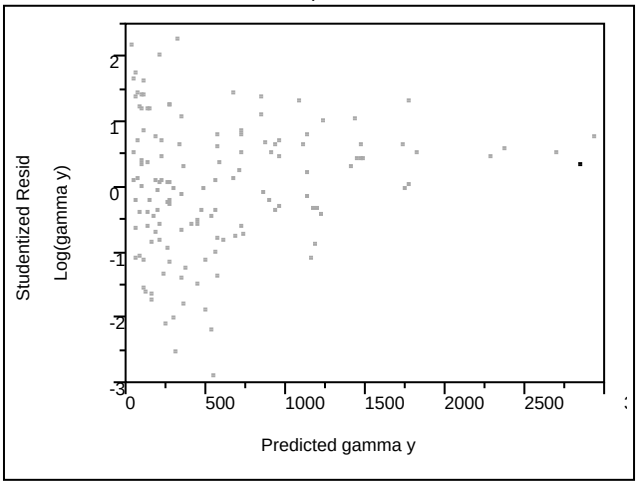
Studentized Resid
Log(gamma y)
2
1
0
-1
-2
-3
0
500
1000
1500
2000
2500
Predicted gamma y

Appendix D: Cross Validation Figures

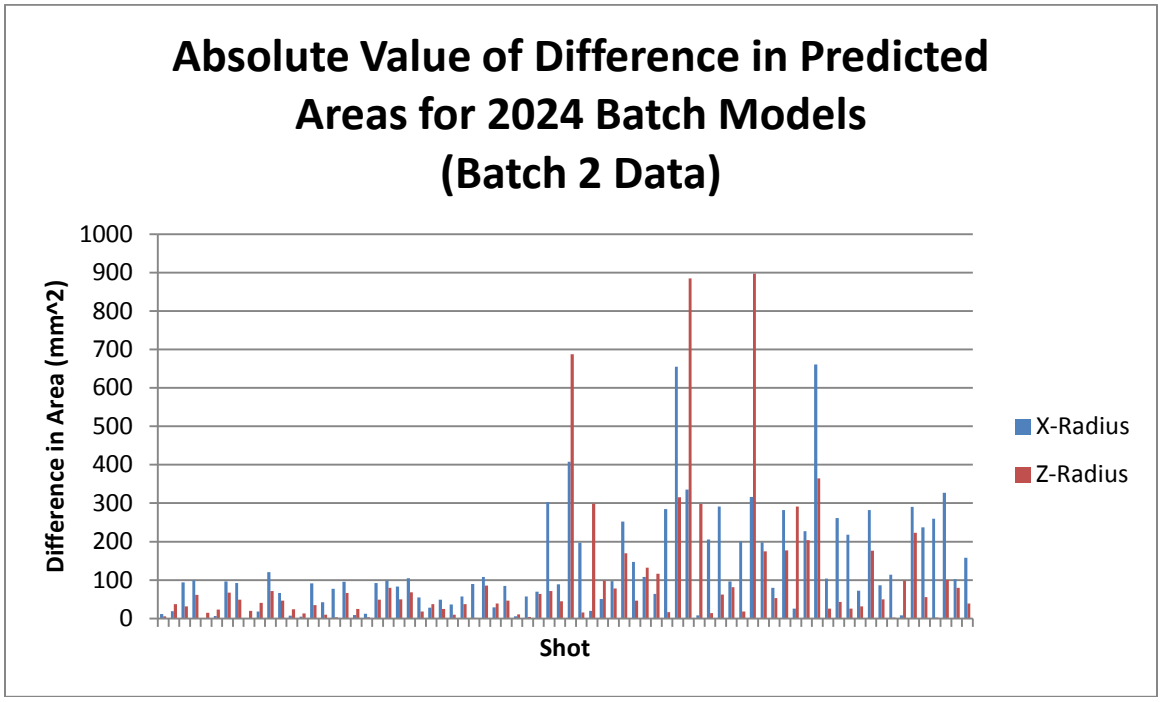

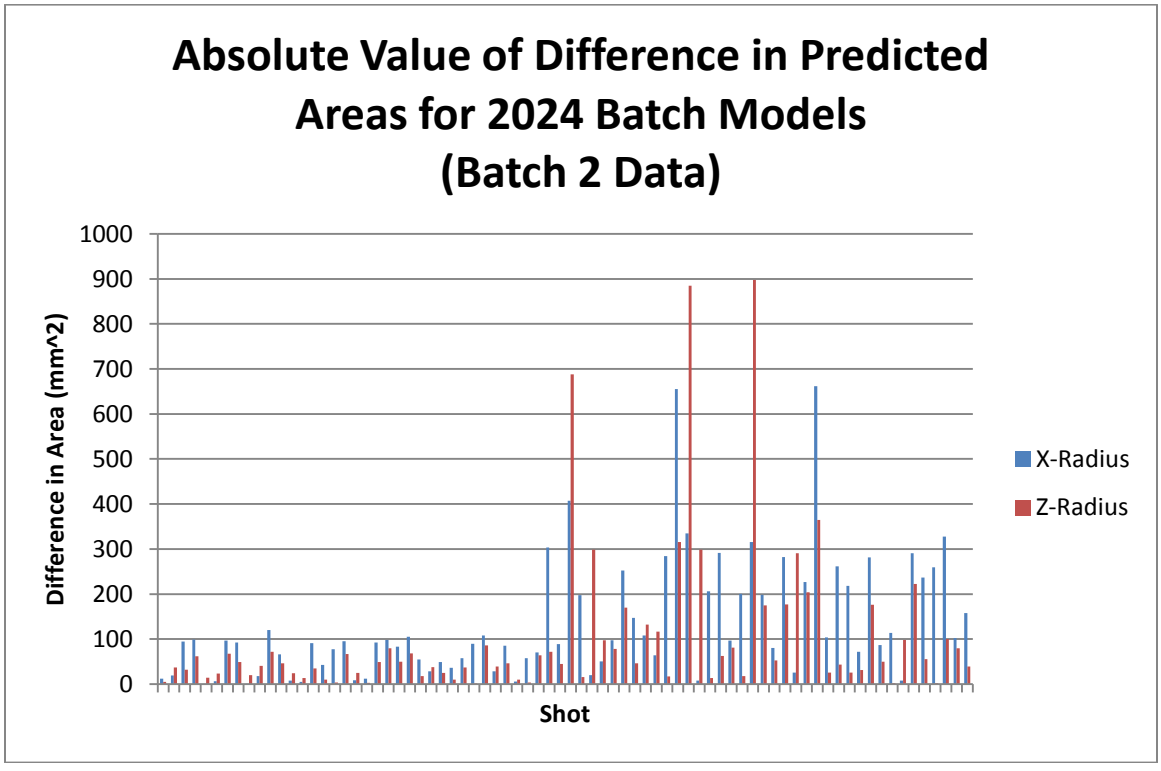

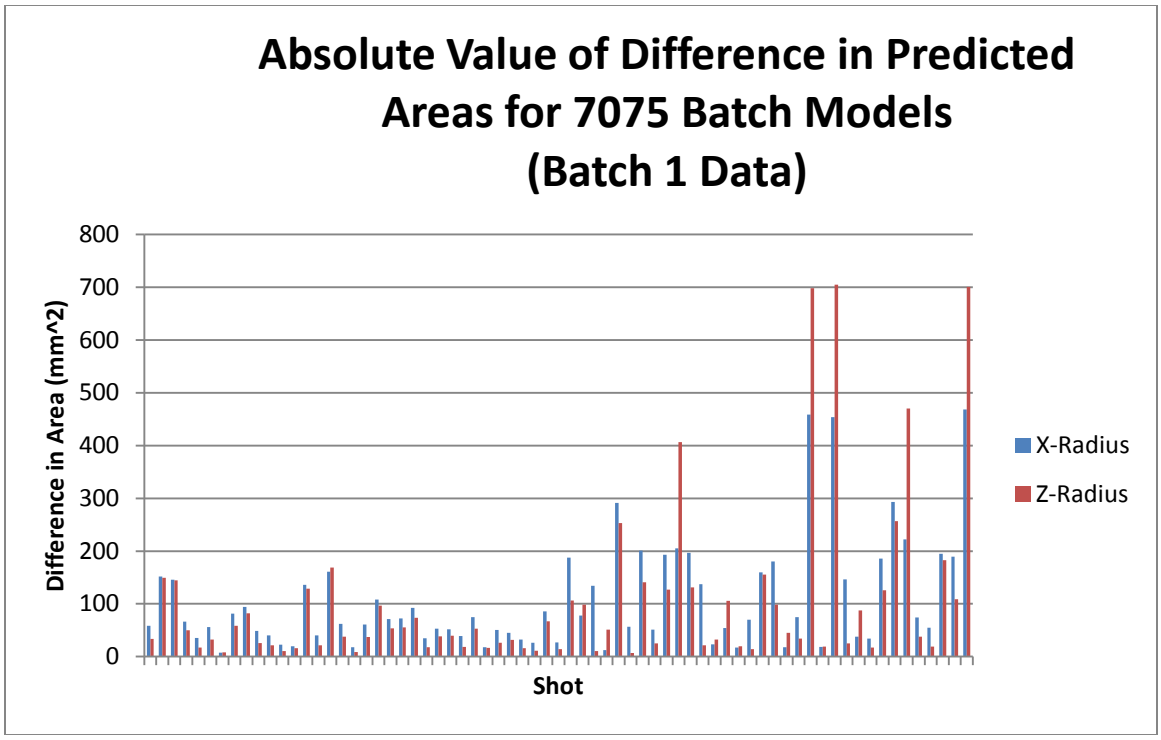
Absolute Value of Difference in Predicted Areas for 7075 Batch Models (Batch 1 Data)
Difference in Area (mm^2)
800
700
600
500
400
300
200
100
0
Shot
X-Radius
Z-Radius

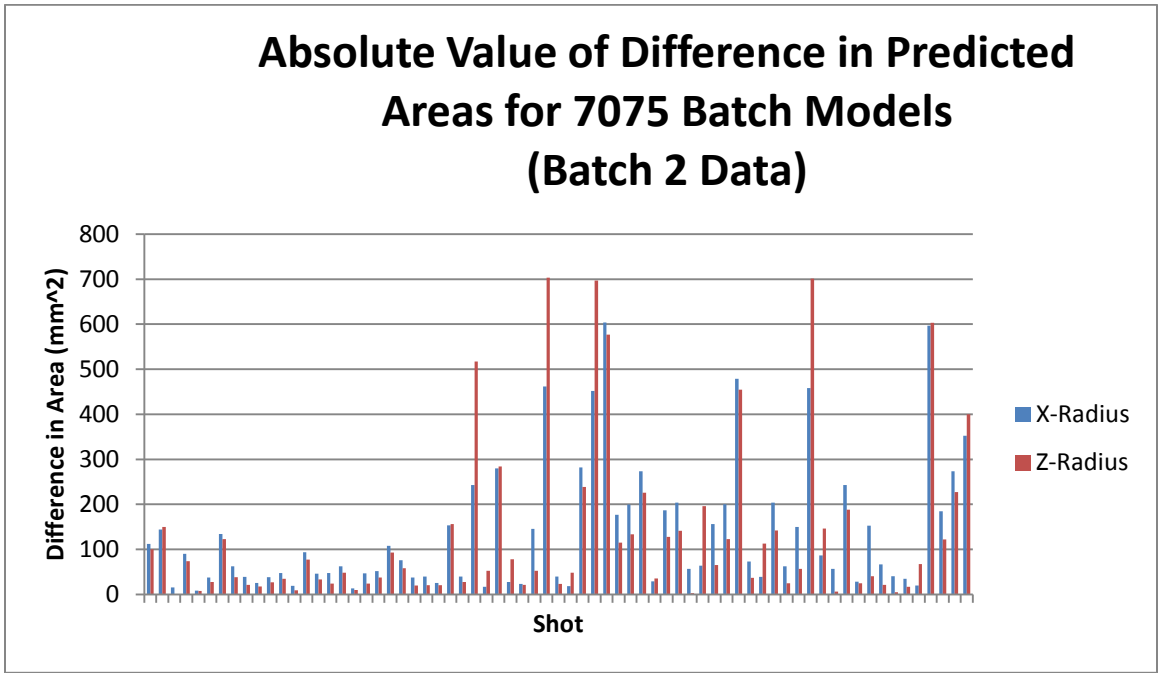
Absolute Value of Difference in Predicted Areas for 7075 Batch Models (Batch 2 Data)
Difference in Area (mm^2)
800
700
600
500
400
300
200
100
0
Shot
X-Radius
Z-Radius

Appendix E: Full Model Validation Charts and Figures

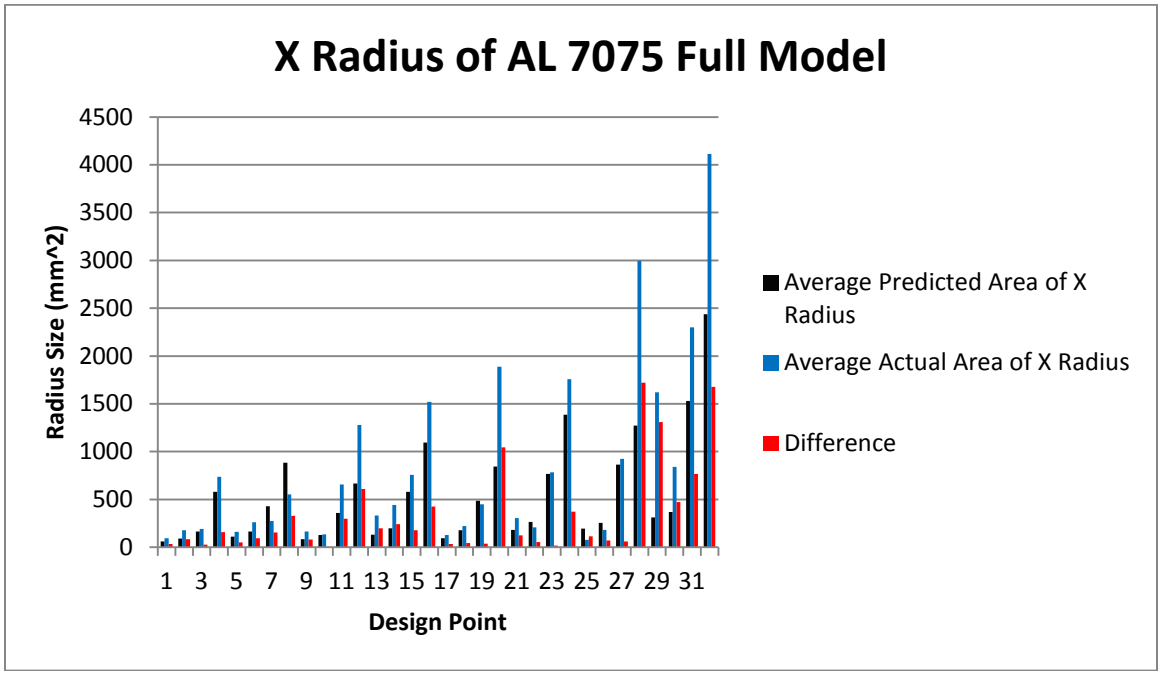

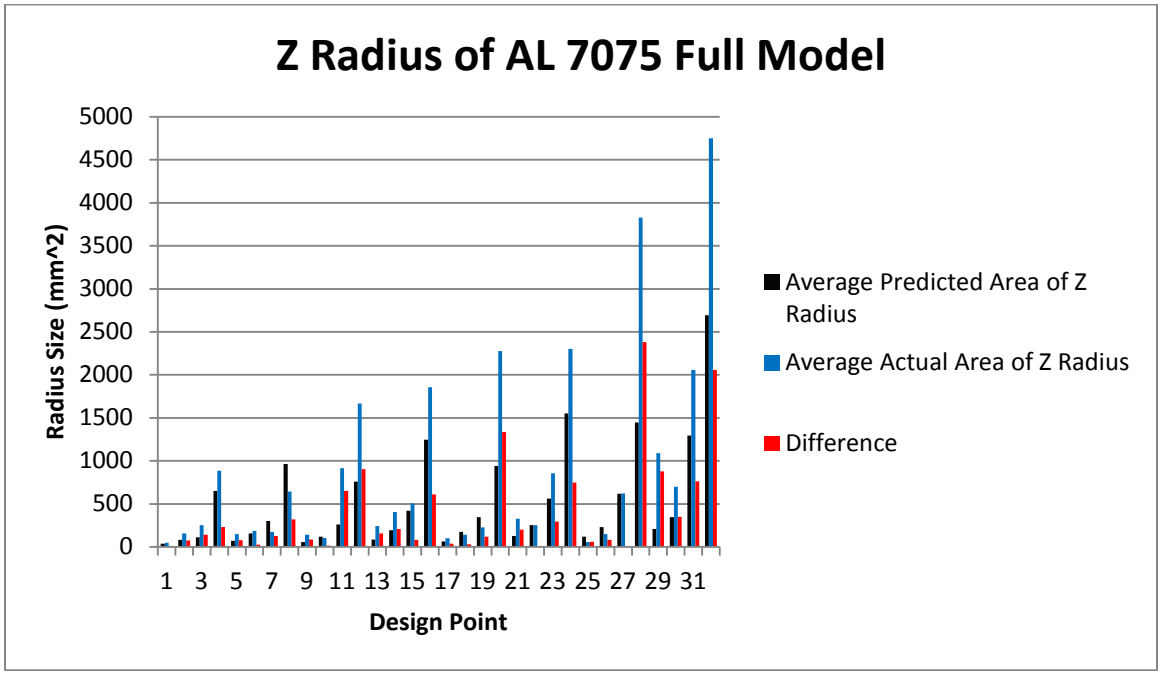

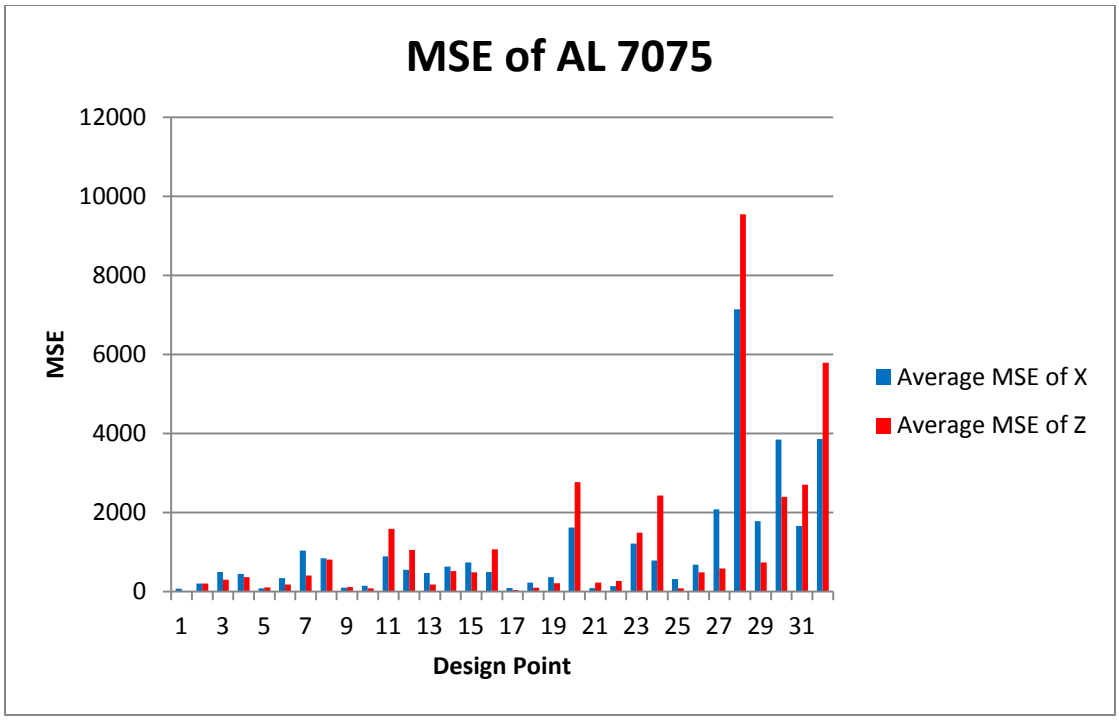
MSE of AL 7075
12000
10000
8000
6000
4000
2000
0
MSE
1 3 5 7 9 11 13 15 17 19 21 23 25 27 29 31
Design Point
Average MSE of X
Average MSE of Z

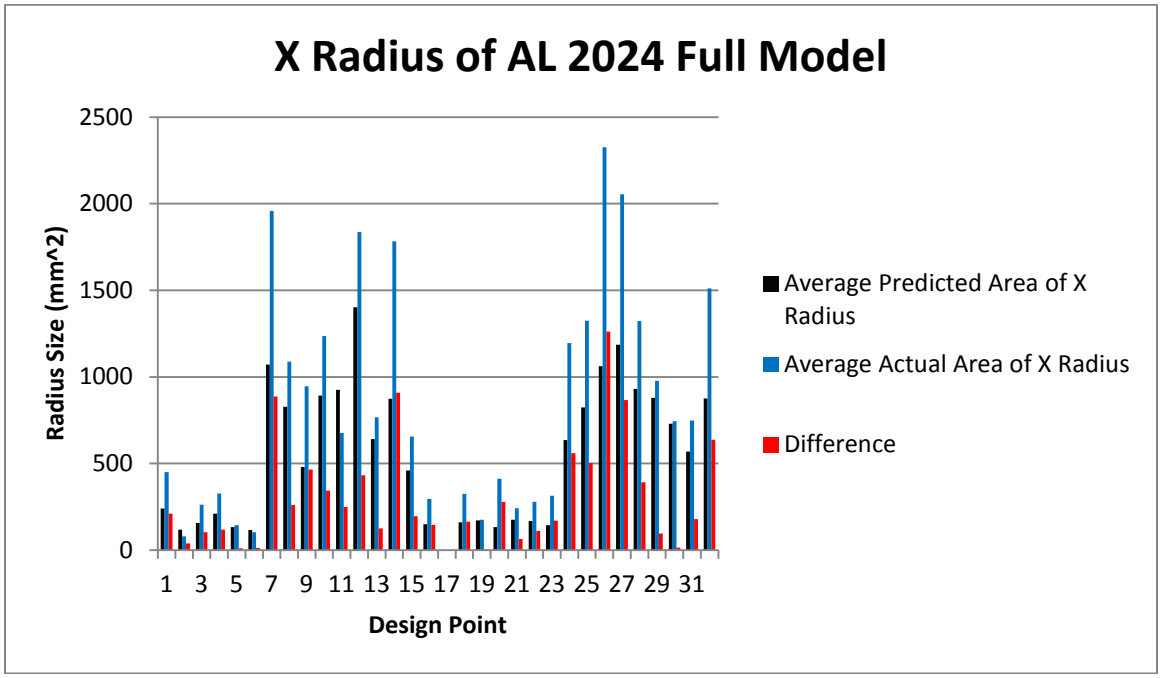
X Radius of AL 2024 Full Model
2500
2000
1500
1000
500
0
Radius Size (mm^2)
1 3 5 7 9 11 13 15 17 19 21 23 25 27 29 31
Design Point
Average Predicted Area of X Radius
Average Actual Area of X Radius
Difference

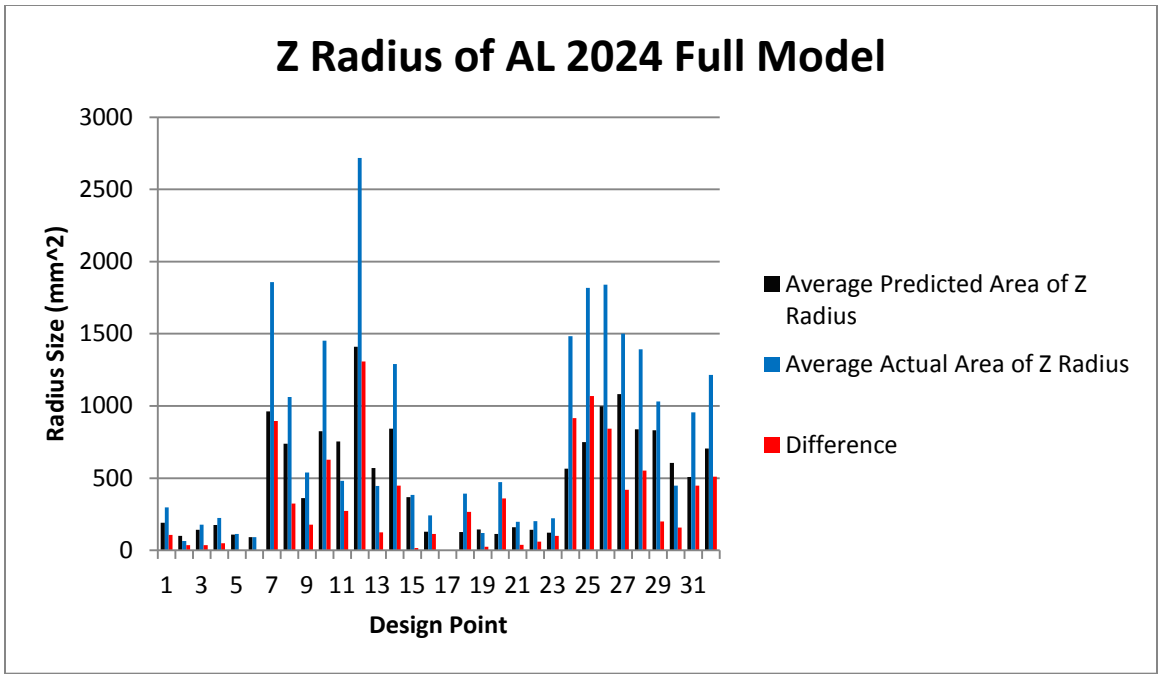
Z Radius of AL 2024 Full Model
Radius Size (mm^2)
3000
2500
2000
1500
1000
500
0
1 3 5 7 9 11 13 15 17 19 21 23 25 27 29 31
Design Point
Average Predicted Area of Z Radius
Average Actual Area of Z Radius
Difference

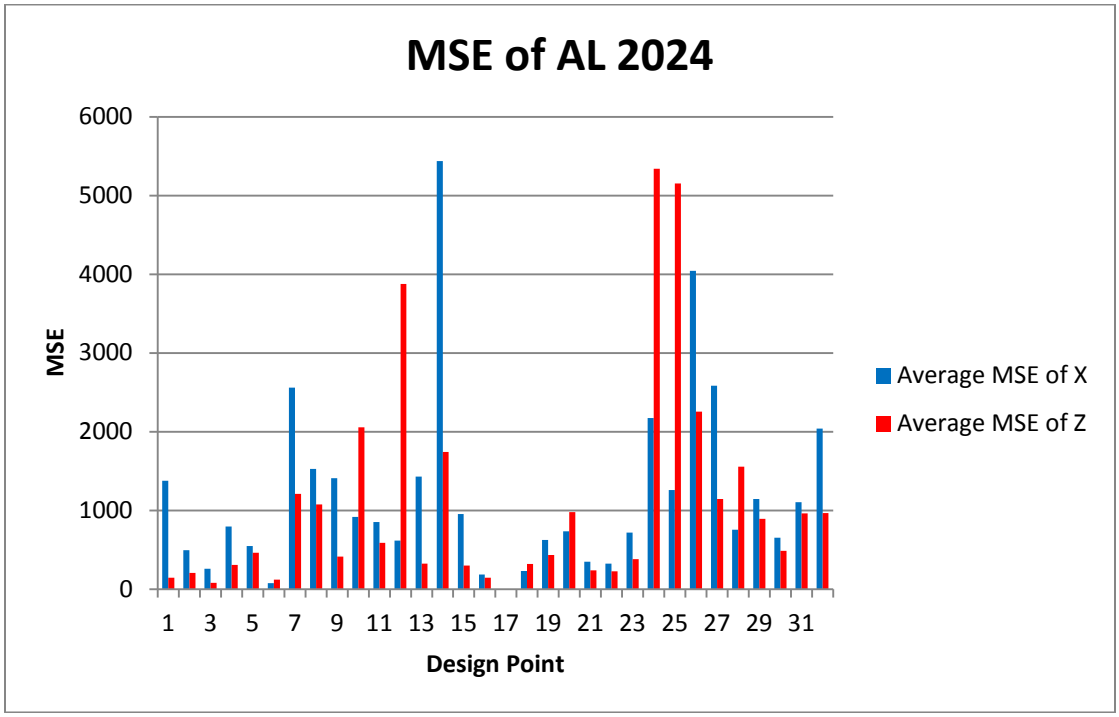
MSE of AL 2024
MSE
6000
5000
4000
3000
2000
1000
0
1 3 5 7 9 11 13 15 17 19 21 23 25 27 29 31
Design Point
Average MSE of X
Average MSE of Z

Works Cited

1. Ball, R. E. (2003). *The Fundamentals of Aircraft Combat Survivability Analysis and Design (Second Edition).* American Institute of Aeronautics and Astronautics.

2. Bestard, J. J., & Kocher, B. (2010). *Ballistic Impact Flash Characterization.* AIAA-2010-2573.

3. Bestard, J., "Survivability Assessments: The Fire Prediction Model (FPM)." *Aircraft Survivability* (Spring 2011): 6-8.

4. Blythe, R. M. (1993). *Preliminary Expirical Characterization of Steel Fragment Projectile Penetration of Graphite/Epoxy Composite and Aluminum Targets.* MS thesis, Air Force Insitute of Technology, Wright-Patterson AFB, Ohio.

5. Henninger, T. A. (2010). *Characterization of Ballistic Impact Flash: An Initial Investigation and Methods Development.* MS thesis, Air Force Institute of Technology, Wright-Patterson AFB, Ohio.

6. Knight, E. E. (1992). *Predicting Armor Piercing Incendiary Projectile Effects After Impacting Composite Material.* MS thesis, Air Force Institute of Technology, Wright-Patterson AFB, Ohio.

7. Lanning, J. W. (1993). *Predicting Armor Piercing Incendiary Projectile Effects After Impacting Two Composite Material.* MS thesis, Air Force Institute of Technology, Wright-Patterson AFB, Ohio.

8. Montgomery, D. C., Peck, E. A., & Vining, G. G. *Introduction to Linear Regression Analysis* (Fourth Edition). John Wiley & Sons Inc. 2006.

9. Reynolds, J. K. (1991). *A Response Surface Model for the Incendiary Functioning Characterizations of Soviet API Projectiles Impacting Graphite Epoxy Composite Panels.* MS thesis, Air Force Insitiute of Technology, Wright-Patterson AFB, Ohio.

10. Talafuse, T. P. (2011). *Empirical Characterization of Ballistic Impact Flash.* MS thesis, Air Force Institute of Technology, Wright-Patterson AFB, Ohio.

REPORT DOCUMENTATION PAGE

Form Approved
OMB No. 074-0188

1. REPORT DATE *(DD-MM-YYYY)*	2. REPORT TYPE	3. DATES COVERED *(From – To)*
09-09-2012	**Master's Thesis**	Sep 2010 – Sep 2012

4. TITLE AND SUBTITLE
BALLISTIC FLASH CHARACTERIZATION OF ENTRY-SIDE FLASH

5a. CONTRACT NUMBER

5b. GRANT NUMBER

5c. PROGRAM ELEMENT NUMBER

6. AUTHOR(S)
Peyton, David J.

5d. PROJECT NUMBER

5e. TASK NUMBER

5f. WORK UNIT NUMBER

7. PERFORMING ORGANIZATION NAMES(S) AND ADDRESS(S)
Air Force Institute of Technology
Graduate School of Engineering and Management (AFIT/EN)
2950 Hobson Street, Building 642
WPAFB OH 45433-7765

8. PERFORMING ORGANIZATION REPORT NUMBER
AFIT-OR-MS-ENS-12-21

9. SPONSORING/MONITORING AGENCY NAME(S) AND ADDRESS(ES)
46th TG OL-AC
Attn: Mr. Jaime Bestard
2700 D Street, Bldg 1661 DSN: 785-6302 x231
WPAFB OH 45433 e-mail: Jaime.bestard@wpafb.af.mil

10. SPONSOR/MONITOR'S ACRONYM(S)
46th TG OL-AC

11. SPONSOR/MONITOR'S REPORT NUMBER(S)

12. DISTRIBUTION/AVAILABILITY STATEMENT
APPROVED FOR PUBLIC RELEASE; DISTRIBUTION UNLIMITED.

13. SUPPLEMENTARY NOTES

14. ABSTRACT
Aircraft survivability is a broad subject that encompasses many fields and subjects. An important part of aircraft survivability is fire prevention. Flashes created by ballistic impacts are a very real threat to aircraft because they can start fires or cause explosions. In an effort to better protect against these flashes, this study seeks to further the understanding and characterization of them.

Recent research on this subject has been greatly helped by the use of high-speed video footage of flash events. This footage has led to new algorithms and methodologies for how to characterize a flash. A preliminary predictive model of a flash event has already been made, but needs to be refined before implementation. This research effort is dedicated to further refining and developing this predictive model by finding a new time series model that more aptly describes the shape of the analyzed data. To this end, new data have been created and analyzed, and a new predictive flash model has been created. This model has been validated and proven to be adequate. Even though there is some amount of work that can still be done to enhance it, it is recommended that this model be implemented into the current flash prediction tools.

15. SUBJECT TERMS
Survivability, ballistic impact flash, Weibull, meta-model

16. SECURITY CLASSIFICATION OF:			17. LIMITATION OF ABSTRACT	18. NUMBER OF PAGES	19a. NAME OF RESPONSIBLE PERSON
a. REPORT	b. ABSTRACT	c. THIS PAGE			Raymond R. Hill, Ph.D.
U	U	U	UU	77	19b. TELEPHONE NUMBER *(Include area code)* (937) 265-6565, ext. 4314; email: rayomnd.hill@afit.edu

Standard Form 298 (Rev. 8-98)
Prescribed by ANSI Std. Z39-18